

INTERPRETATION OF RADAR IMAGERY FROM
SPACE SHUTTLE COLUMBIA OVER
SOUTHERN ALGERIA AND
SOUTHWESTERN
LIBYA

By

JOSEPH ANDREW ONTKO, JR.

Bachelor of Science in Arts and Sciences

Oklahoma State University

Stillwater, Oklahoma

1978

Submitted to the Faculty of the
Graduate College of the
Oklahoma State University
in partial fulfillment of
the requirements for
the Degree of
MASTER OF SCIENCE
July, 1992

INTERPRETATION OF RADAR IMAGERY FROM
SPACE SHUTTLE COLUMBIA OVER
SOUTHERN ALGERIA AND
SOUTHWESTERN
LIBYA

Thesis Approved:

Gary F. Stewart

Thesis Adviser

Douglas C. Kist

[Faint signature]

Thomas C. Collins

Dean of the Graduate College

ACKNOWLEDGEMENTS

This study was made possible by the generous policy of NASA of disseminating data free of charge to university-affiliated researchers. The SIR-A imagery was received from the NASA National Space Science Data Center. The SIR-A experiment was operated under Principal Investigator Dr. Charles Elachi. The Landsat Thematic Mapper scene was received from the Jet Propulsion Laboratory (JPL) node of the NASA Pilot Land Data System. I am grateful to the JPL for preliminary processing of the Landsat data, and for sending me important JPL publications concerning the SIR-A and SIR-B experiments.

The Landsat data was processed further and viewed at the Oklahoma State University Geography Department Center for Applications of Remote Sensing (CARS). CARS director Dr. Steven Stadler granted use of the CARS processing computer. Mr. Joe Seig, laboratory manager of CARS, spent many hours helping me process, view and photograph the Landsat scene and subscenes.

A special thanks goes to my thesis adviser Dr. Gary F. Stewart, who has provided assistance and guidance throughout my career as a geologist. Dr. John W. Shelton, Dr. Douglas C. Kent and Mr. M. Richard Hackett served as committee members; I am grateful for their assistance. My wife Kathy

offered encouragement and showed patience, for which I am greatly appreciative.

Finally, I would like to acknowledge the geologists who have examined first-hand the geology of the Central Sahara and have reported their findings in various publications. Their descriptions, maps and photographs provided an important framework for this study.

TABLE OF CONTENTS

Chapter	Page
I. SCOPE OF STUDY	1
II. RADAR-IMAGE INTERPRETATION	4
Space-Borne Radar Systems	4
Interpretation of Radar Images	8
Characteristics of the Radar System ..	8
Variables of Surface Terrain	10
Limitations of Radar Imagery	15
Previous Uses of Shuttle Imaging Radar	16
III. GENERAL GEOLOGY OF SOUTHERN ALGERIA AND SOUTHWESTERN LIBYA	18
Basement Complex	19
Paleozoic Erathem	22
Mesozoic Erathem	26
Cenozoic Erathem	26
Pleistocene-Holocene Climate	28
IV. INTERPRETATION OF THREE SIR-A SEGMENTS	30
Ubari Segment, Libya	31
Differentiation of Terrain by Radar Signature	37
Ghat Segment, Libya and Algeria	38
Comparison of SIR-A with Gemini XI Photographs	42
Differentiation of Terrain by Radar Signature	43
Fracture Patterns	45
Tiririne Segment, Algeria	46
Comparison of SIR-A with Landsat Imagery	50
Differentiation of Terrain by Radar Signature	58
Pan-African Stress Regime Implied by Tectonic Elements	61
V. CONCLUSIONS	66
SELECTED BIBLIOGRAPHY	69

Chapter	Page
APPENDIXES	75
APPENDIX A - GLOSSARY OF SELECTED ARABIC TERMS	76
APPENDIX B - MAPS USED IN INTERPRETATIONS	77

LIST OF TABLES

Table		Page
I.	Comparison of Space-Borne Radar Systems	7
II.	Central Saharan Terrains Distinguished by Radar Signature	66

LIST OF FIGURES

Figure	Page
1. Index Map of North Africa with Location of SIR-A Image Strip Investigated	3
2. General Configuration of SIR-A System	9
3. Effect of Flat Terrain and Sloping Terrain upon Local-Incidence Angle	10
4. General Effects of Variation in Slope upon Radar Imagery	11
5. Effect of Microrelief upon Backscatter in Smooth and Rough Terrain	13
6. General, Figurative Effects of Variation in Local-Incidence Angle and Surface Roughness upon Backscatter	14
7. General Geologic Map of the Hoggar-Iforas-Air Basement Complex	20
8. General Geologic Column of Southwestern Libya ...	23
9. Oblique Aerial Photograph of Oasis Gabre Oun	34
10. Close-up Photograph of SIR-A Image of the Messak Escarpment, Wadi Agial and Oases in the Ubari Sand Sea	34
11. Close-up Photograph of SIR-A Image of Ghat and Surrounding Area	40
12. Subset of Southwest Quarter of Landsat Scene, Tiririne Segment, Algeria	48
13. Close-up Photograph of SIR-A, Plate 4, C2	52
14. Landsat Subset of Figure 13	52
15. Close-up Photograph of SIR-A, Plate 4, E3	53
16. Landsat Subset of Figure 15	53

Figure	Page
17. Close-up Photograph of SIR-A, Plate 4, G3	55
18. Landsat Subset of Figure 17	55
19. Close-up Photograph of SIR-A, Plate 4, K4	56
20. Landsat Subset of Figure 19	56
21. Landsat Subset of "Crypto-Volcanic" Feature in Plate 4, L3	58
22. Plan View of Hypothesized Pan-African Stress Regime in Southern Algeria and Northern Niger, with Tectonic Elements Observed in the Hoggar and Air Massifs	63

CHAPTER I

SCOPE OF STUDY

Whereas the geology of many areas on Earth has become well known through extensive study and field-mapping, some vast, remote areas are poorly understood. Imagery of these remote areas taken from Space facilitates reconnaissance, and permits the formation of many useful working hypotheses. The tentative explanations form a vital framework for detailed study, which could be carried out by use of larger scale aerial photographs and by geologic field-mapping.

Photographs from manned space missions, Landsat images, and other satellite images provide an extensive database from which geologic reconnaissance can be conducted. Since 1978 a limited amount of radar imagery from Space has become available. Radar imagery is substantially different from conventional photographic and scanned images. A detailed understanding of its acquisition and unique capabilities, as well as appreciation of its limitations, are required for proper interpretation.

Radar imagery over the remote North African Central Sahara, acquired from the Space Shuttle in 1981, is interpreted in this study. The single 50-km-wide strip of imagery covers a variety of types of terrain across the

highly complex basement rocks of the Hoggar Massif in southern Algeria, and across the sedimentary rocks and sand seas along the northwestern margin of the Murzuk basin in southwestern Libya (Figure 1; Plate 1). Rocks are well exposed in this hyperarid region, providing optimal conditions for remote sensing of geology. The radar-imagery strip selected is about 1650 km long and 50 km wide, covering more than 80,000 sq km. Three image segments, each covering about 10,000 sq km, were selected for detailed interpretation. Two of these segments cover parts of the northwestern flank of the Murzuk basin; the third covers a section of the Hoggar Massif (Plate 1). Several photographs from the Gemini XI space mission were used as ancillary data to evaluate southwestern Libya, and a Landsat Thematic Mapper scene was used in interpretation of radar imagery of the Hoggar Massif.

Although the geology of the region has been described by numerous worthy investigators, the vastness and remoteness of the area, and the hostile environment have precluded definitive understanding. This study attempts to demonstrate the usefulness of small-scale radar imagery in development of a better understanding of this remote region. Radar signatures of the various types of terrain are differentiated, and the radar imagery is compared with conventional imagery from Space. The work of previous investigators was essential to and integrated with interpretations presented here.

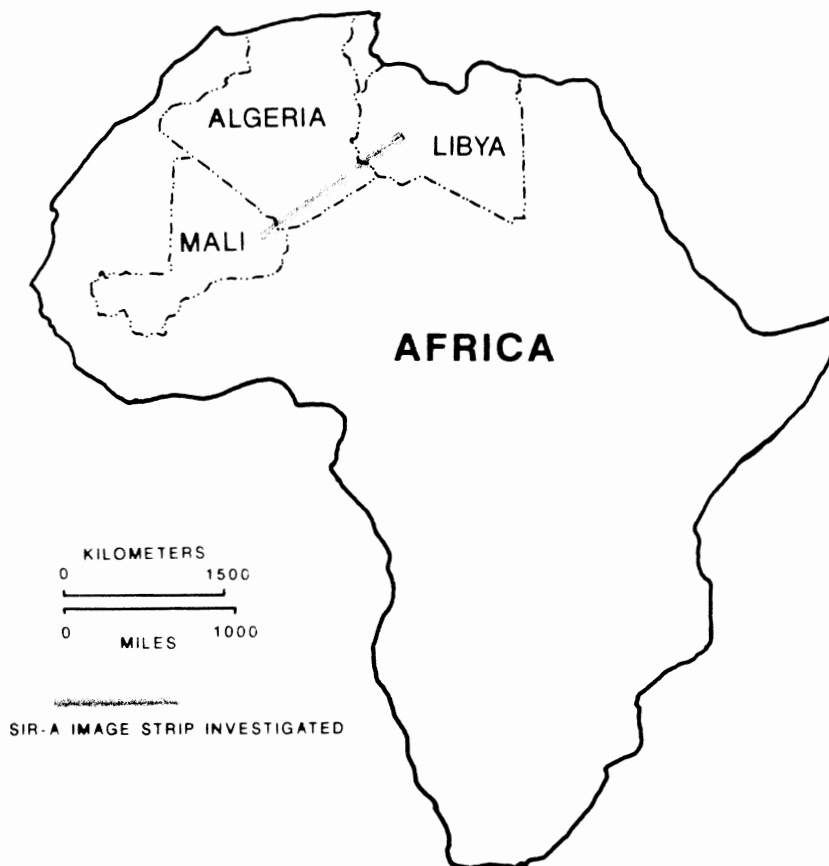


Figure 1. Index Map of North Africa with Location of SIR-A (Shuttle Imaging Radar-A) Image Strip Investigated.

CHAPTER II

RADAR-IMAGE INTERPRETATION

The Side Looking Airborne Radar (SLAR) system was developed in the early 1950's for military reconnaissance. Following declassification, its unique capabilities were found of great use in mapping of terrain, for which it has been utilized heavily since the late 1960's. Radar (radio detection and ranging) is restricted to the wavelength spectrum between approximately 1 mm and 1 m, and for wavelengths of more than 3 cm is unaffected by cloud cover, rain, smoke and other atmospheric "clutter," which often render conventional aerial photographs and scanner images useless. Radar is an active system, emitting its own energy; it is unaffected by lighting conditions, allowing acquisition of imagery at night. The first complete maps of nearly perpetually cloud-covered Panama were made from SLAR imagery in 1968; a similarly successful project covering the cloudy Amazon Basin was completed in the early 1970's, during which several previously unknown large rivers were discovered (Lillesand and Kiefer, 1987, p. 474).

Space-Borne Radar Systems

SLAR generally is operated from conventional aircraft,

but in 1978 the Seasat SAR satellite was placed into orbit, becoming the first Space-borne radar system (Lillesand and Kiefer, 1987, p. 476). Designed primarily to study oceanic phenomena such as currents and waves, Seasat was useful in analysis of terrain. During its three and one half months of operation imagery was acquired over most of North America and adjacent oceans. The first Space mission specifically designed for terrain mapping from radar imagery was the second flight of the Space Shuttle Columbia, launched November 12, 1981; it was referred to as the Shuttle Imaging Radar-A (SIR-A) experiment. The mission was considered a success, even though its planned duration of four days was shortened to two and one half days. Radar imagery of more than 10 million square kilometers was acquired from diverse terrains between 41 degrees North and 35 degrees South latitude. Among the discoveries, SIR-A was found able to penetrate 2 m into the dry, wind-blown sand sheets of the southwestern Egyptian desert; an intricate network of previously unknown buried drainage channels was revealed, indicating a previous, wetter climate (Cimino and Elachi, 1982, p. 4-1).

SIR-A was a synthetic-aperture radar-imaging system (SAR), which through a complex processing routine synthesized the effect of an antenna much longer (as much as 600 m) than its actual size (9.35 m x 2.16 m). This allowed useful resolution at long ranges and high altitudes. The radar signal was sent from a planar antenna mounted on the

SIR-A pallet assembly in the Shuttle bay, was reflected from the Earth's surface then received by the antenna. The time delay and Doppler history of the returns were recorded on optical film onboard. The holographic signal film was processed at the Jet Propulsion Laboratory on an optical correlator, where the synthetic aperture was formed. From this the final image was produced on film, from which photographic prints can be made (Cimino and Elachi, 1982, p. 2-5). This study utilizes a selection of these photographic prints "painted" by the SIR-A system, from data take 29-30.

The SIR-A experiment was followed by the SIR-B experiment operated from Space Shuttle Challenger (mission 41-G), October 5-13, 1984 (Cimino, Holt and Richardson, 1988). This radar system was modified from the SIR-A equipment to allow digital data recording, from which images could be enhanced and manipulated digitally, and to allow multiple angles of incidence, from which stereoscopic images and quantitative elevation models were produced. Unfortunately, antenna-power problems limited data acquisition to less than half that planned. A sophisticated large-format camera (LFC) taking conventional photographs also was operated during mission 41-G. Overlapping coverage allows stereoscopic imaging of these high-resolution photographs. A north-south strip of the LFC photographs was taken that crosses the SIR-A image strip examined in this study near the Algerian-Libyan border; however, 70% cloud cover precluded use of the photographs in this study (and

this fact illustrates a critical advantage of radar imagery). Table I shows the characteristics of the three Space-borne radar systems described above.

TABLE I
COMPARISON OF SPACE-BORNE RADAR SYSTEMS
(Modified from Cimino et al., 1988, p. 4-6)

	<u>Seasat</u>	<u>SIR-A</u>	<u>SIR-B</u>
SYSTEM PARAMETERS			
Wavelength	23.5 cm	23.5 cm	23.5 cm
Average incidence angle	23 deg	47 deg	15-60 deg
Polarization	HH	HH	HH
IMAGE PARAMETERS			
Swath width	100 km	50 km	20-40 km
Azimuth resolution	25 m	40 m	25 m
Range resolution	25 m	40 m	17-58 m
ORBITAL PARAMETERS			
Average altitude	795 km	260 km	224-354 km
Inclination	108 deg	38 deg	57 deg
DATA COLLECTION			
Coverage (million sq km)	100	10	5
Optical data	-----	8 hours	8 hours
Digital data	40 hours	-----	7 hours
MISSION STATISTICS			
Launch date	6-27-78	11-12-81	10-5-84
Duration	3.3 mos	2.4 days	8.3 days
Platform	Satellite	Columbia	Challenger
Flight		STS-2	41-G

SIR-C is planned for a future Space Shuttle mission and new radar satellites are being scheduled by the European Space Agency, Japan and Canada as well as the United States

(Cimino, Holt and Richardson, 1988, p. 4). Since August 10, 1990 the Magellan spacecraft has been imaging perpetually cloud-covered Venus with synthetic-aperture radar. Fascinating images of domed structures, impact craters, volcanoes and extensive fracture-systems are being scrutinized (unpublished annotated images from the Jet Propulsion Laboratory). During its mission Magellan is expected to cover about 80% of the planet, providing detailed imagery for mapping of the previously hidden surface.

Interpretation of Radar Images

The radar image is a representation of the strength of the signal return, referred to as "backscatter". Variation in backscatter is displayed through a spectrum of gray scales with zero backscatter shown as black and increasingly greater backscatter shown in progressively lighter shades of gray; white indicates return of all emitted energy. The SIR-A images are processed in 16 levels of gray. Digital radar data can be assigned colors based on the degree of backscatter or other variables, but analog radar imagery is black and white; no radar imagery can depict real surface-color in the manner that the photographic process can. Because radar imaging is substantially different from optical sensing, an understanding of the radar-surface interaction is necessary for proper interpretation of images (Lillesand and Kiefer, 1987, p. 472).

Characteristics of the Radar System

Backscatter is a function of characteristics of the radar system and properties of the surface terrain.

The two major characteristics of the system are wavelength and look angle. Wavelengths resolve surface roughness. Wavelengths of Seasat, SIR-A, and SIR-B are each 23.5 cm (L Band), but look angles vary. The look angle is measured from the radar beam to the vertical (Figure 2). The resultant antenna-incidence angle is about 3 degrees greater than the look angle, due to curvature of the Earth. The resultant antenna-incidence angle of the SIR-A system

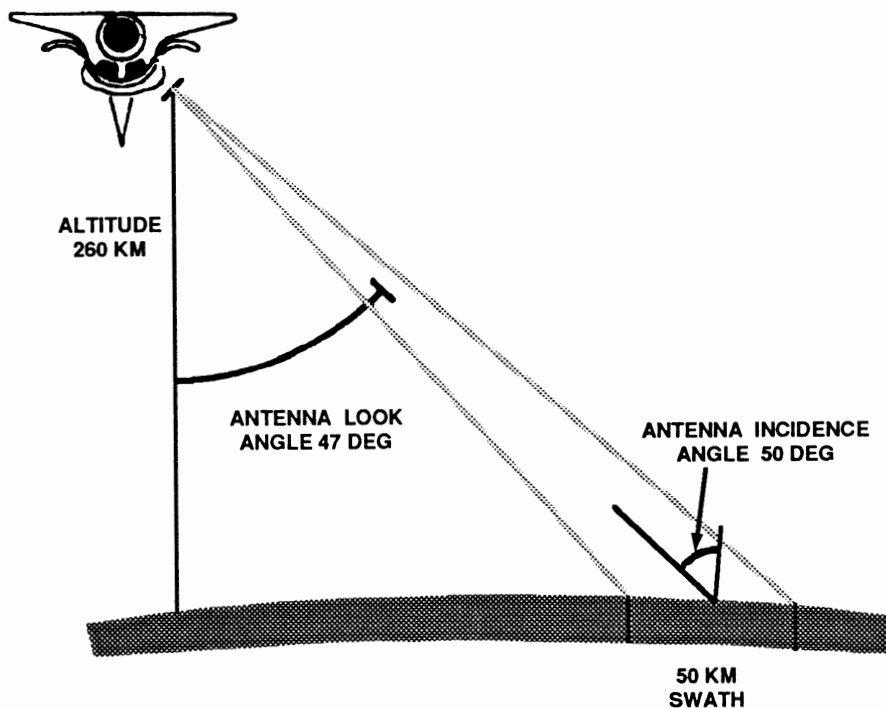


Figure 2. General Configuration of SIR-A System (Modified from Cimino, Holt and Richardson, 1988, p. 5).

varied from 50 degrees at the northward (downrange) edge of the image to 44 degrees at the southward edge. Wavelength and antenna look angle of the SIR-A system were not adjustable (Cimino and Elachi, 1982).

Variables of Surface Terrain

Attributes of terrain that affect backscatter are topography, small-scale surface roughness, and soil moisture (Sabins, 1983, p. 2077).

Radar backscatter is dominated by the local-incidence angle, which is a function of the antenna-incidence angle and topographic slope. For flat terrain, the local-incidence angle is equal to the antenna-incidence angle (Figure 3A). For sloping terrain, the local-incidence angle occurs between the radar beam and perpendicular bisect of the slope (Figure 3B). With an increasing local-incidence

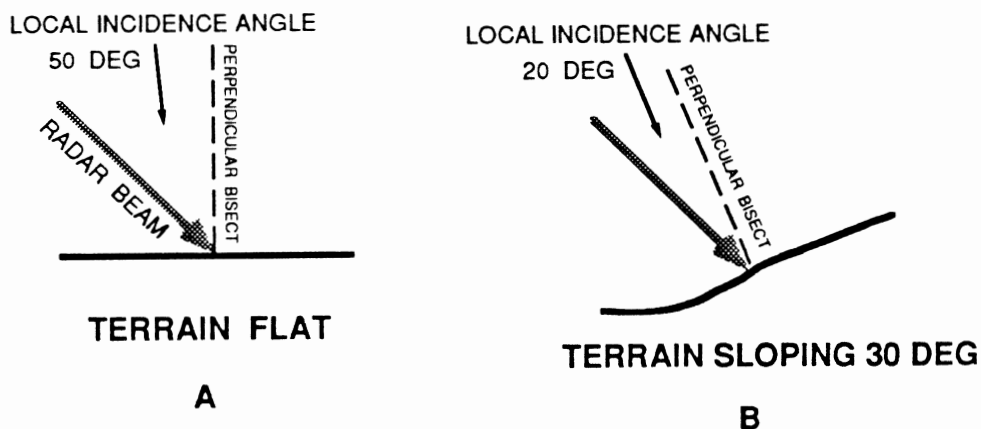


Figure 3. Effect of Flat Terrain (A) and Sloping Terrain (B) upon Local-Incidence Angle.

angle (terrain sloping away from antenna) radar energy is increasingly reflected away from the antenna, and darker images appear. Terrain-slopes facing the radar beam decrease the local-incidence angle and return more backscatter; this produces brighter images (Figure 4) (Lillesand and Kiefer, 1987, p. 494).

High-relief terrain may introduce a distortion in the radar image called "layover". In this case the radar beam reaches the peak of a hill or mountain before reaching the base, resulting in an image in which the peak appears in front of its base. Layover is particularly severe in Seasat imagery (23-degree antenna-incidence angle), but the larger 47-degree average antenna-incidence angle of SIR-A produces layover only on slopes greater than 47 degrees, which are sparse in most terrains.

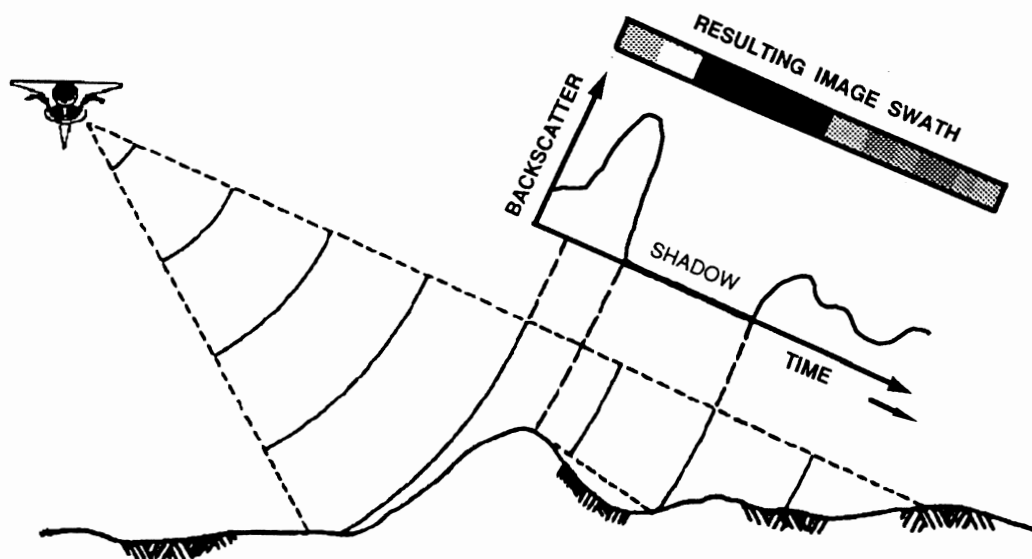


Figure 4. General Effects of Variations in Slope upon Radar Imagery (Modified from Lillesand and Kiefer, 1987, p. 495).

Small-scale roughness refers to microrelief of the ground surface, measured in centimeters. Roughness can be calculated using the modified Rayleigh scattering criterion formulas (Lillesand and Kiefer, 1987, p. 495):

$$H_r = \frac{\text{radar wavelength}}{25 \cos I} \quad \text{Rough Criterion}$$

$$H_s = \frac{\text{radar wavelength}}{4.4 \cos I} \quad \text{Smooth Criterion}$$

where I is the local-incidence angle and H is the height of the root-mean-square of the microrelief. Although the local-incidence angle may vary from 0 to 90 degrees, the calculation is made here for non-sloping terrain, for which the antenna-incidence angle equals the local-incidence angle.

For SIR-A imagery H_r is 8.3 cm, and H_s is 1.5 cm. On non-sloping smooth terrain (microrelief < 1.5 cm), such as calm water and desert sand, the signal is reflected specularly, away from the antenna, resulting in a very dark or black image (Figure 5A). On rough terrain (microrelief > 8.3 cm), such as coarse gravel, trees and brush, the signal is diffused and a bright return is recorded (Figure 5B). Microrelief between 1.5 and 8.3 cm will be viewed in intermediate shades of gray. Over sloping terrain the local-incidence angle varies, changing H_r and H_s , which in

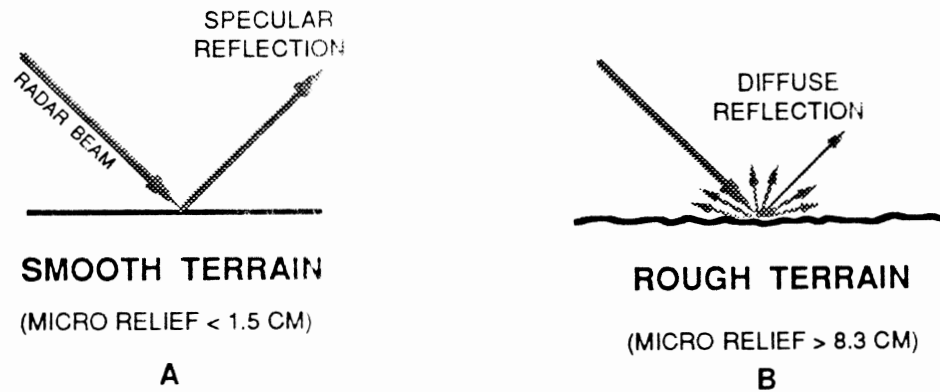


Figure 5. Effect of Microrelief upon Backscatter in Smooth and Rough Terrain.

turn alters the amount of backscatter. The general effects of varying local-incidence angle and surface roughness on backscatter are shown figuratively in Figure 6. At a low-incidence angle the smooth surface returns the most backscatter, whereas the rough surface diffusely reflects some of the radar energy away from the antenna. But at a higher angle the smooth surface reflects most of the radar energy away from the antenna, resulting in a very dark or black image, whereas the rough surface still returns some backscatter (Cimino, Holt and Richardson, 1988, p. 5).

One additional circumstance, generally limited to urban areas, is that of the corner reflector: the radar beam is reflected from the corner of a building and may actually be amplified, producing an extremely bright signature. Offshore oil platforms and ships at sea commonly produce corner reflections (Lillesand and Kiefer, 1987, p. 497).

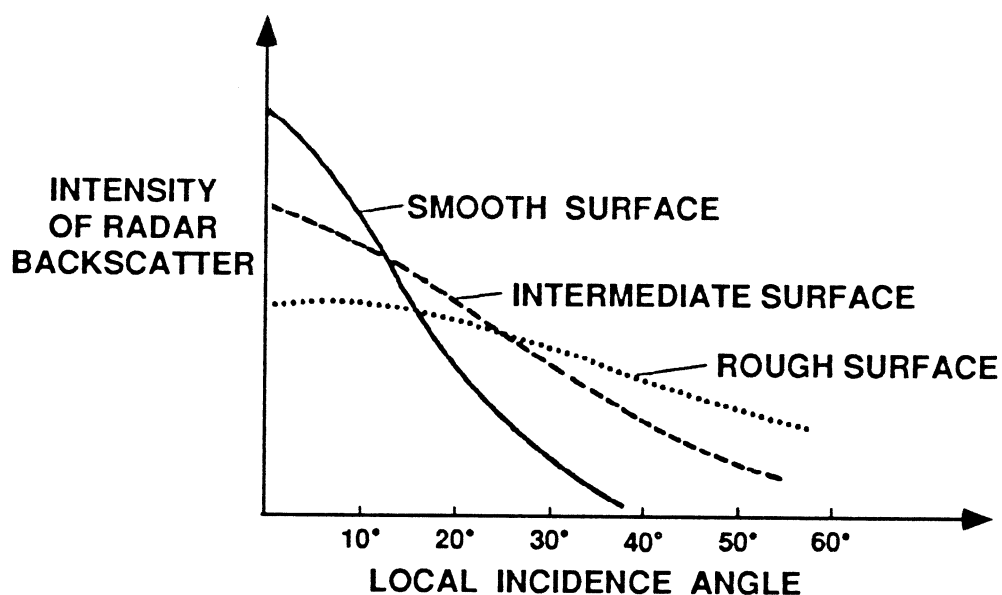


Figure 6. General, Figurative Effects of Variation in Local-Incidence Angle and Surface Roughness upon Backscatter (Modified from Cimino, Holt and Richardson, 1988, p. 5).

Moisture in sand, soil, rocks and vegetation increases the complex dielectric constants of these materials, a measure of the electrical characteristics of matter. Increase in dielectric constant increases radar return. This effect generally is minor and thus is masked by topography and surface-roughness (Sabins, 1983, p. 2077). In hyperarid regions, such as the Sahara Desert, the dielectric constant is very low, allowing the radar signal to penetrate as much as several meters of sand.

Vegetation generally is a strong radar reflector, being classed as a rough surface according to the above formulas

(for SIR-A). The contour of the vegetal canopy generally conforms to the underlying topography; relative to vegetated terrain, images may be brighter and somewhat enhanced over nonvegetated smooth terrain. Drainage patterns detectable through heavily vegetated areas commonly are greatly enhanced in radar images: effects of tall stands of trees against smooth water are similar to corner reflectors.

Limitations of Radar Imagery

As with most conventional aerial photographs, there is scale distortion in radar imagery that limits its use in orthographic mapping. Detailed comparison of a SIR-A image segment with topographic maps over eastern North Carolina disclosed an azimuth (along flight path) scale of very nearly 1:500,000, whereas the range (across flight path) scale varied nonlinearly and averaged 1:463,000 (Cimino and Elachi, 1982, p. 4-51). The results of this scale comparison are generally in agreement with the SIR-A imagery over Algeria and Libya examined in this study; however, the detail of available topographic maps was scant.

A look direction within about 30 degrees of the orientations of lineaments and other extended features tends to subdue or even eliminate the features from a radar image, whereas features perpendicular to radar illumination generally are enhanced. This selective enhancement of lineaments has also been observed on Landsat images in which the sun-illumination direction is similar to the radar look

direction. The shorter lineaments are more likely to be subdued (Ford, 1980, p. 2083; Cimino and Elachi, 1982, p. 4-30). Any quantitative study of lineaments should employ at least two separate images with illumination directions at least 30 degrees apart.

The resolution of the radar system is an obvious limitation. From a field experiment, resolution of the SIR-A system was determined to be about 40 m; however, a 3 m wide by 1.5 m deep canal was faintly visible in the North Carolina SIR-A image, indicating that features smaller than the stated resolution can be detected under certain circumstances (Cimino and Elachi, 1982, p. 2-8 and 4-51).

The SIR-A system was unable to calibrate absolute backscatter. Backscatter was also found to be nonlinear. These two factors will limit quantitative studies of backscatter (Cimino and Elachi, 1982, p. 2-11 and 2-20).

Previous Uses of Shuttle Imaging Radar

Shuttle imaging radar has been of great use in evaluation of a wide variety of terrains in different climates around the world. In many studies, terrains are classified according to their radar signatures and correlated to lithology of outcropping rock, structural geology and geomorphology. Sabbins (1983) distinguished six types of terrain (carbonate, clastic, volcanic, alluvial and coastal, melange and metamorphic) in a geologic interpretation of SIR-A imagery of Indonesia. In imagery

over the Egyptian eastern desert, five major lithologic units were distinguishable in SIR-A imagery: wadis, Nubian Sandstone, granitic plutons, country rocks and ultramafic rocks (Cimino and Elachi, 1982, p. 4-2). The first four of these types of terrains were distinguished in the imagery examined in this study.

Prior to the Space Shuttle, one of the greatest uses of imaging radar was in mapping cloud-covered humid regions. SIR-A was very useful in evaluating hyperarid terrains. In Landsat and other conventional imagery, the high reflection of visible and infrared light from sand-covered areas creates a low-contrast image with great reduction of detail. However, radar imagery commonly shows much more detail.

Shuttle imaging radar has been used in archaeological studies. SIR-B and LFC photographs were used to trace ancient roads in the desert of southern Oman, which led to the discovery of what may be the lost city of Ubar, covered by sand about A.D. 100 ("The Sunday Oklahoman," 1992).

The response of radar to surface roughness has been helpful in evaluating volcanic terrain. Aa lava generates images much brighter than those of pahoehoe lava. Individual lava flows, pyroclastic cones, dikes and other elements of volcanic terrains were also differentiated (Ford et al., 1986, p. 41; Cimino and Elachi, 1982, p. 4-19).

CHAPTER III
GENERAL GEOLOGY OF SOUTHERN ALGERIA
AND SOUTHWESTERN LIBYA

Sand seas cover only a portion of the Central Sahara. Large areas of Precambrian, Paleozoic and Mesozoic rocks are exposed (Plate 1), which were described first by early French and Italian explorers. Geologic studies accelerated with the discovery of oil in Libya in the late 1950's. Although many studies remain confidential, the Petroleum Exploration Society of Libya published numerous informative guidebooks in the late 1960's. Conant and Goudarzi (1967) produced the first concise English-language summary of the geology of Libya. Goudarzi (1970) presented a more detailed overview in a U. S. Geological Survey professional paper. Following the second symposium on the geology of Libya, held at Tripoli in 1980, several papers were published in the three-volume set of records: The Geology of Libya. This investigator participated in an extensive proprietary report of the petroleum geology of Libya in 1990 and 1991, which inspired him to study further the fascinating geology of this area.

Lelubre (1952) completed the first regional investigation of the Hoggar Massif of southern Algeria. The

more recent works of Bertrand and others (1976, 1978, 1986), and Black et al. (1979) provide insights to the tectonic history of this extremely complex area by integration of information from geochronological, lithostratigraphic and structural investigations.

Although much has been learned about the geology of the Central Sahara, its remoteness and hostile environment have maintained it as a "frontier" area, with much opportunity for additional study.

Basement Complex

The Hoggar Massif in southern Algeria with its extensions, Iforas (eastern Mali) and Air (northern Chad), cover a very large area (Plate 1). The Hoggar, Iforas and Air are composed mostly of Precambrian metamorphic and igneous rocks. They have undergone a series of orogenies which has resulted in extremely complex terrain. Massive north-trending fault zones, some traceable along the entire 750-km exposure, divide the basement outcrop into genetically distinctive Eastern, Central and Western belts (Figure 7). Some fault zones are mylonitic and as much as 4 km wide (Schurmann, 1974, p. 104). Many of the faults have been reactivated during successive orogenies. Bertrand et al. (1986) interpreted some faults in the Central belt as deep-seated thrusts, some of which are judged to have evolved into strike-slip faults, right-lateral and left-lateral. Folds commonly are associated with the faults.

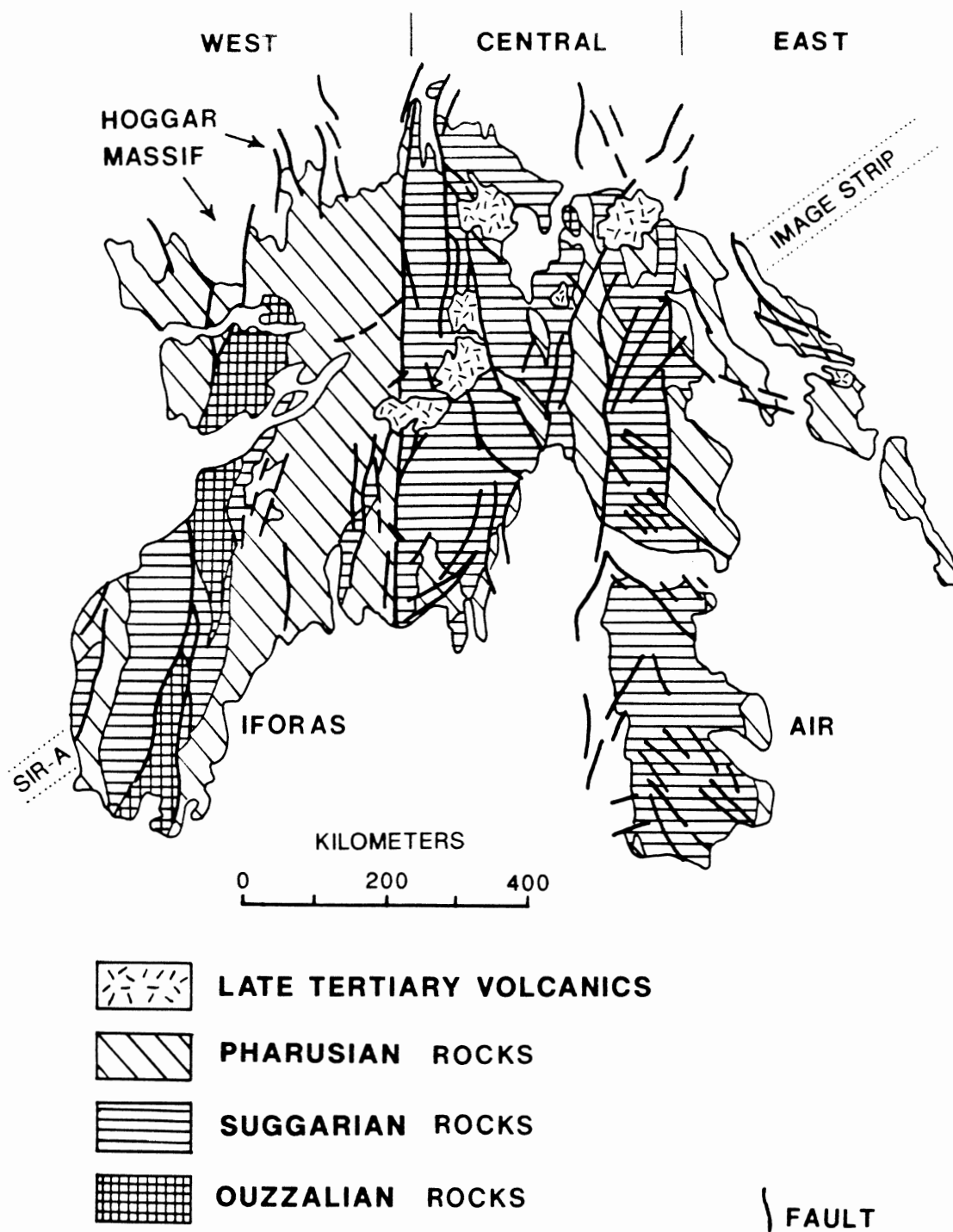


Figure 7. General Geologic Map of the Hoggar-Iforas-Air Basement Complex (Modified from Bankwitz et al., 1968, p. 461).

The oldest rocks, Precambrian Ouzzalian granulites and charnockites, are exposed in a narrow north-south zone in the Western Hoggar belt and extend into the Iforas area (Figure 7). They have been dated between 2800 and 3300 m.y. old. In contact with Ouzzalian rocks are Suggarian gneisses, granites and banded high-grade metasediments. Suggarian rocks are genetically related to the Eburnean orogeny, dated about 2000 m.y. (Figure 7). They crop out in the Central and Western Hoggar belts in high-grade metamorphic facies of granulite to amphibolite (Carpena et al., 1988; Lancelot et al., 1976; Allegre and Caby, 1972; Ferrara and Gravelle, 1966).

Pharusian low-grade metavolcanic and metagraywackes are predominantly in the Western and Eastern belts, but are also in the Central belt, in narrow linear zones. The Pharusian has been divided locally into upper and lower groups. Although age of the Pharusian is not known accurately, it post-dates Suggarian rocks and is of a lower-grade greenschist facies (Bertrand et al., 1978, p. 956; Lelubre, 1952).

Granitic plutons, dated between 515 and 670 m.y., were emplaced throughout much of the Hoggar-Iforas-Air Massif before, during and after the Pan-African orogeny (Allegre and Caby, 1972; Boissonnas et al., 1969). Bertrand et al. (1986) recognized the Pan-African event as an almost-complete tectonometamorphic reworking of rocks in the Central Hoggar belt, where only small areas of Suggarian

rocks are unmodified. The Pan-African orogeny is recognized throughout much of North Africa and is dated about 600 m.y.; it has been associated with continental collision (Bertrand et al., 1986; Ghuma and Rogers, 1980; Black et al., 1979).

The Late Paleozoic Hercynian epeirogeny mildly affected some parts of the Hoggar Massif; mylonites from some fault zones have been dated at 250 m.y. (Schurmann, 1974, p. 102). Apatites in Eburnean carbonatites of the Western Hoggar belt were overprinted by two later thermal events. A strong thermal event, dated 500-630 m.y., corresponded to the Pan-African orogeny, and a weaker event, dated 247-263 m.y., recorded the Hercynian epeirogeny (Carpena et al., 1988).

Paleozoic Erathem

Cambro-Ordovician quartzitic sandstones of the Gargaf Group crop out in broad aprons of gently dipping strata around the periphery of the Hoggar Massif, around much of the Tibesti uplift, and are exposed on the Gargaf arch (Plate 1). The type locality is at the Gargaf arch. The Cambro-Ordovician sandstones are remarkably consistent in lithology throughout the North African Sahara (Goudarzi, 1970, p. 24) and are divided into four formations. These sandstones are about 900 m thick on the eastern flank of the Hoggar Massif, a highland known as the Tassili N'Ajjer (Plate 1), where they are highly fractured and dip eastward into the Murzuk basin (Burdon, 1980, p. 600; Massa et al., 1972). Figure 8 shows a general geologic column of

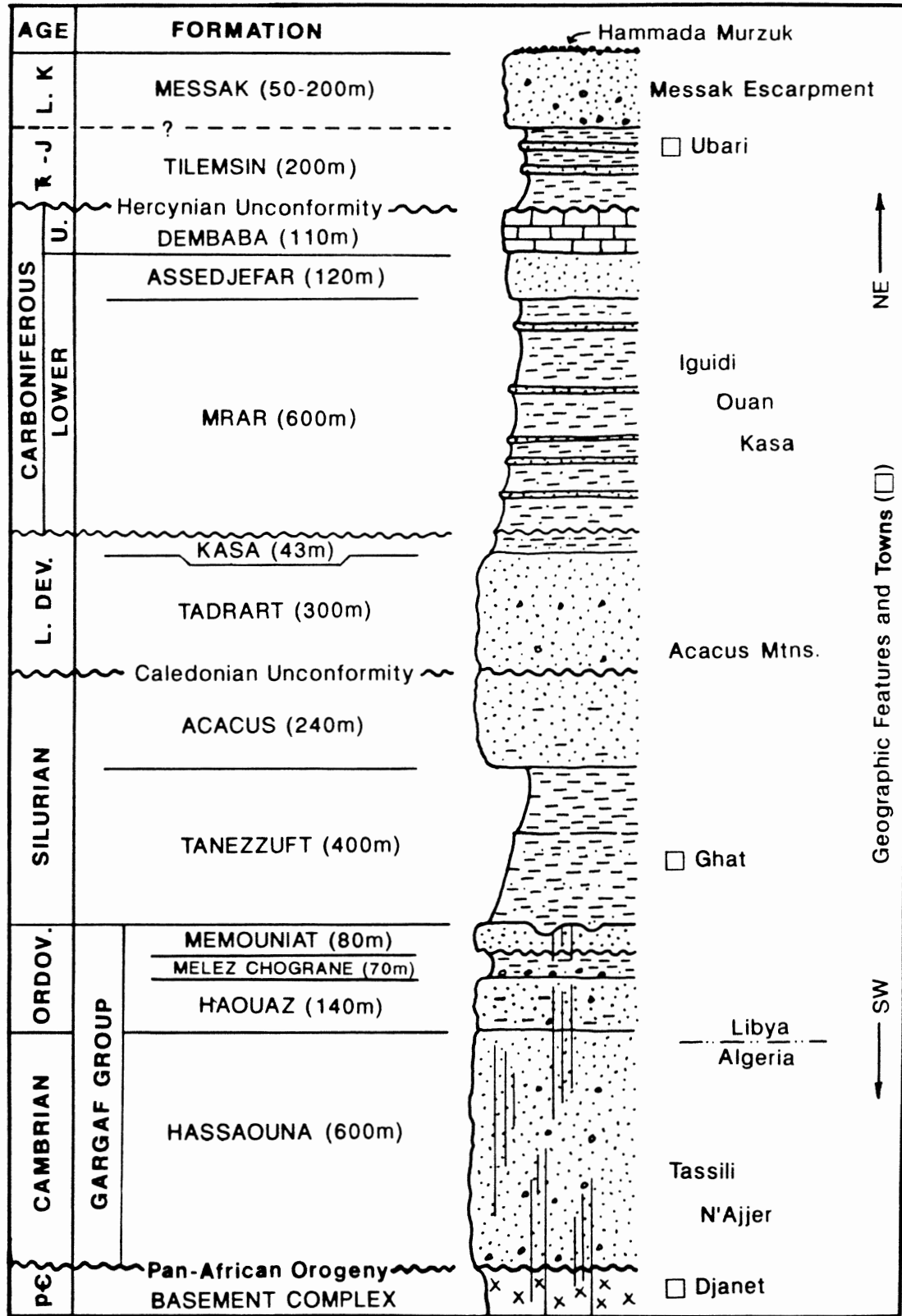


Figure 8. General Geologic Column of Southwestern Libya.

Paleozoic and Mesozoic rocks and their thicknesses expected along the SIR-A image path in southwestern Libya. A crude cross section, with geographic features and towns, is shown by turning the column 90 degrees clockwise.

Glacial striations, chatter marks, scoured paleovalleys and roches moutonnées are carved on the Cambro-Ordovician sandstones around the periphery of the Hoggar Massif. In aerial photographs of 1:50,000 scale, roches moutonnées are visible at some localities and paleovalleys observed in the Tassili N'Ajjer are as long as 10 km, as wide as 1-2 km, and as deep as 400 m (Beuf et al., 1969, p. 107-108).

Following extensive Late Ordovician - Early Silurian glaciation, the first widespread Paleozoic marine transgression inundated the central Sahara; during this event the Tanezzuft Shale (Figure 8) was deposited. At Klitzsch's (1969) type section of the Silurian and Devonian, 35 km southeast of Ghat (Plate 1), the Tanezzuft is 402 m thick. The lower half is composed of shale with interbeds of fine grained sandstone, whereas the upper half is made up of bituminous shales that were source rocks for the oil and gas fields of western Libya and eastern Algeria.

Overlying the Tanezzuft Shale is the Upper Silurian Acacus Sandstone (Figure 8). Klitzsch (1969, p. 86) measured 345 m of Acacus at the type section, but the sandstone thins to the north and is absent over the Gargaf arch, an effect of the Late Silurian Caledonian epeirogeny.

Above the Caledonian unconformity are the Tadrart

Sandstone and the Kasa Shale, measured at 315 m and 43 m respectively by Klitzsch (1969, p. 87); both are Lower Devonian. Although Upper Devonian rocks crop out near the southwestern margin of the Murzuk basin and are in the subsurface of the Ghadames basin in northwestern Libya, they are absent on the northwestern flank of the Murzuk basin. The Acacus and Tadrart sandstones form the Acacus Mountains (Plate 1), a prominent, highly dissected cuesta that dips eastward into the Murzuk basin. A north-trending strike valley has formed in the Tanezzuft Shale between the west face of the Acacus escarpment and the Cambro-Ordovician sandstones of the Tassili N'Ajjer to the west.

Carboniferous rocks have been described in exposures northwest and south of the Gargaf arch (Whitbread and Kelling, 1982; Goudarzi, 1970, p. 27-28). Carboniferous rocks dominantly are shale with interbedded sandstones; they form a broad valley between the Acacus Mountains and Messak escarpment (Plate 1) where they are mostly covered by the sands of Iguidi Ouan Kasa, but they are estimated to be as thick as 800 m. The Upper Carboniferous Dembaba Limestone is sparsely exposed along the lower slopes of the Messak escarpment (Grunert and Busche, 1980, p. 852).

The Gargaf, Acacus, Tadrart and Carboniferous sandstones are important oil and gas reservoirs in western Libya and eastern Algeria, and the Gargaf is an important aquifer in the same area. A large deposit of iron ore is in Carboniferous rocks in the southern margin of the Gargaf.

Mesozoic Erathem

Mesozoic rocks form a prominent escarpment around the northern and western margins of the Murzuk basin. About 200 m of Triassic/Jurassic Tilemsin shales and interbedded sandstones (Figure 8) form the lower slopes of the escarpment. Grunert and Busche (1980) observed that landslide deposits compose most of the slopes in the western portion of the escarpment. The Tilemsin is capped by 50-200 m of Messak Sandstone, which commonly forms cliffs along the escarpment. The Messak is a facies of the widespread Upper Jurassic and/or Lower Cretaceous Nubian Sandstone, also known as the Sarir Sandstone (Lorenz, 1987; Klitzsch and Baird, 1969). Above the escarpment the Messak forms a wide hamada (rocky plateau) around much of the Murzuk basin.

The Nubian (Messak) sandstones are important oil and gas reservoirs in the Sirte basin of east-central Libya. They are also one of the most important and widespread aquifers in the country.

Cenozoic Erathem

Late Tertiary-Quaternary alkalic basaltic lavas have been mapped in central and northeastern portions of the Hoggar Massif (Plate 1) (Bordet, 1952). Basement topography was elevated as much as 1000 m beneath these volcanic complexes, presumably from Pliocene doming prior to extrusion. Mt. Tahat of the Atakor volcanic complex, 40 km north of Tamanrasset, rises to 3003 m, the highest point in

the Hoggar. The rise of magma probably was facilitated by deep-seated faults in the vicinity of the magma reservoirs (Black and Girod, 1970, p. 203). Morten et al. (1980) examined one of the lava complexes northwest of Djanet. They dated one basaltic lava flow with an irregular columnar structure at 8.4 m.y.; this flow was overlain by a flow with a globular, pseudo-pillow structure having concentric cracks and dated at 6.8 m.y.

Late Tertiary volcanism was widespread in the Central Sahara; it occurred in the Tibesti Mountains of northern Chad and in west-central Libya, as well as in the Hoggar Massif (Goudarzi, 1970, p. 42; Vincent, 1970).

Tertiary sedimentary rocks are sparse in southern Algeria and southwestern Libya. Tertiary lacustrine limestones are exposed in small areas south and west of the Gargaf arch, and lie on portions of the Messak Sandstone along the northern margin of the Murzuk basin (Goudarzi, 1970, p. 41).

Quaternary sand dunes and sheets cover several large areas in southwestern Libya. The two largest sand seas are the Ubari Sand Sea south and west of the Gargaf arch and north of the Messak escarpment, and the Murzuk Sand Sea which covers much of the Murzuk basin (Plate 1). Iguidi Ouan Kasa, between the Acacus Mountains and the Messak escarpment, and Erg D'Admer, along the southeastern margin of the Hoggar Massif, are smaller sand seas. Wadis and other low-relief areas are also commonly covered by sand.

Elevations of southern Algeria and southwestern Libya are moderate. In the Hoggar Massif elevations average 1000 to 1500 m. The highest points of the Tassili N'Ajjer are about 1800 m; the Acacus Mountains near Ghat are about 1400 m above sea level. The town of Ghat, in the Tanezzuft valley, is about 660 m above sea level. The Hamada Murzuk averages 800 m, and the lowest area is along Wadi Agial, at about 400 m.

Pleistocene-Holocene Climate

Abundant archaeological, stratigraphic, and geomorphic evidence indicates that the Central Saharan climate was much wetter during the Pleistocene and early Holocene. Bordet (1951) described as many as eight zones of laterite in Late Tertiary basalts of the Hoggar, which indicated subtropical conditions existed. Kubiena (1955) discussed brown loams that cap the basalt; he concluded that the loams were formed under tropical to subtropical climatic conditions.

Grunert and Busche (1980), and Busche (1980) determined that the Messak escarpment and large landslides along its frontal slopes developed under wet conditions during the Pleistocene. Maley (1977) correlated early Holocene alternating wet and dry periods with sedimentation, erosion and Paleolithic and Neolithic culture.

Bones of elephant, giraffe, antelope and other subtropical to tropical fauna associated with fluvial and lacustrine deposits have been dated between 1440 and 5475 BC

(Pachur, 1980, p. 785). Drawings and carvings of these same fauna on cliffs of Acacus, Tadrart and Messak sandstone have similar dates (Graziosi, 1969; Mori, 1969). Extensive ruins and many ancient graves along Wadi Agial and other areas of the Fezzan (southwestern Libya) attest to a hospitable climate during the early and middle Holocene (Daniels, 1969; Graziosi, 1969).

The numerous drainage valleys carved through the Hoggar Massif, Tassili N'Ajjer, Acacus Mountains and Hamada Murzuk now rarely contain more than sand. The current average annual rainfall is between 5 and 10 mm. Many parts of the region receive no rainfall for several consecutive years. The rain that does eventually fall generally occurs locally as torrential downpours. Summer temperatures are consistently well over 100 degrees F. Nights are relatively cool; winter night-time temperatures near or below freezing are not uncommon. Prevailing wind from the northeast and southwest is a dominant agent of erosion, and is the dominant force in shifting of sand dunes and in violent sand storms (Goudarzi, 1970, p. 15).

CHAPTER IV

INTERPRETATION OF THREE SIR-A SEGMENTS

Each of the three segments selected for interpretation covers about 50 km X 200 km; locations of segments are shown in Plate 1. Each segment is named by the major town within it. One plate has been prepared for each segment, which includes a photograph of the original radar image received from NASA, and an interpretation that outlines the major types of terrain and selected features, such as faults, oases and towns (see Plate 2, for example). The photographs have numbers and letters along the left and bottom edges, respectively, to aid in location of features. The scale of the photographs is 65% of the original imagery, resulting in an azimuth scale (along flight path) of approximately 1:770,000 (0.65 cm = 5 km), and an average range scale (across flight path) of approximately 1:712,000. The range scale varies from bottom to top of the photographs, and it is not linear. Elevations selected from Defense Mapping Agency (DMA) topographic maps are shown on the interpretations (line drawings). Synthesized information from maps (Appendix B), books and papers has been integrated into the interpretations. Appendix A contains a glossary of selected local Arabic terms used to describe various

landforms common to the Sahara.

The length (flight path) of the image strip is oriented about N57E. Due to variation in latitude along the orbital path, each segment has a slightly different orientation. The look direction (illumination direction) is from the bottom of the image, along which the reference letters appear (Plate 2). Slopes facing the bottom of the image generally are brightly imaged, whereas slopes facing away from the bottom tend to be darker or in shadow.

Ubari Segment, Libya

The Ubari segment (Plate 2) covers a portion of the northern margin of the Murzuk basin, which is rimmed by the Messak Sandstone. The Ubari Sand Sea lies north of the Messak Sandstone outcrop. The look direction across this image segment is approximately N32W.

The Messak Sandstone is imaged in the southwest half of this SIR-A segment (Plate 2). It forms a broad hamada ("hamada" is an Arabic term meaning "rocky plateau" (Appendix A)) dipping gently southward into the Murzuk basin, and is of Late Jurassic and/or Early Cretaceous age (Lorenz, 1987 and 1980; Klitzsch and Baird, 1969). A prominent escarpment, clearly defined in the image, has formed along the northern edge of the Messak (G5 to P1). Although the escarpment slope faces away from the look direction, its image is bright with very little shadowing, indicating a slope less than the look angle and a rough

surface. Grunert and Busche (1980) observed numerous landslides along the western Messak escarpment. Although the image of a portion of the western escarpment slope (not shown) is brighter and wider than the Ubari segment, minor landslides may have occurred along portions of the northern escarpment. In a photograph (Klitzsch and Baird, 1969, p. 78) the escarpment slope appears to be about 30 degrees. This is less than the average radar look angle (47 degrees), allowing its imaging; however, shadows are along some portions of the escarpment, indicating slopes steeper than the radar look angle. Klitzsch and Baird (1969) stated that escarpment relief is 160 m south of Germa (K3), where they measured 55 m of Messak Sandstone underlain by 105 m of Tilemsin shale and interbedded sandstones; the lowermost portion of the Tilemsin was covered.

Another photograph in Klitzsch and Baird (1969, p. 69), near the escarpment edge, shows the surface of the Messak Sandstone as very rocky; this corresponds well with a bright image over Messak terrain, which is referred to locally as the Hamada Murzuk. Numerous dendritic drainage systems, clearly imaged, extend generally southeastward across the Messak Sandstone into the Murzuk basin (Plate 2).

The southern margin of the image is very dark, indicating reflection from a smooth surface (G1-M1). A geologic map (Muller-Feuga, 1954, Plate 5) shows evidence that this dark area is a sarir (gravel plain) covering the Messak Sandstone. Average size of gravels of the sarir must

be small (less than 1.5 cm), because the surface returned little backscatter.

The northeast half of the image is covered by the Ubari Sand Sea, which is underlain by Carboniferous rocks (Klitzsch and Baird, 1969, p. 68). The smooth surface of the sand reflected nearly all radar energy away from the antenna, which produced a very dark to black image. Numerous linear sand dunes, 5 to 18 km long, are apparent in the far northeast portion of the image (N to P, 3 to 5). One group is oriented about N65E, and a second group is oriented approximately N35E. They are enhanced due to their orientation generally perpendicular to the radar look direction. Relief of some of these sand dunes is as much as 150 to 200 m (Muller-Feuga, 1954, Plates 19 and 20; Goudarzi, 1970, p. 17).

About 13 scattered bright spots are within the Ubari Sand Sea (for example N3). Most or all of these are oases, some of which correspond to oases mapped by Muller-Feuga (1954, Plate 6). Photographs of oases Oum El Ma (N3), Maharouga (O3), and Gabre Oun (P3) in Muller-Feuga (1954, Plates 20 and 22) show small lakes surrounded by palm groves. A second photograph of Gabre Oun is shown in Goudarzi (1970, p. 17) and reproduced here as Figure 9. The radar images of Oum El Ma and Gabre Oun clearly show a dark area (small lake) surrounded by a bright rim (palm trees), which corresponds well to the photographs. These oases are shown in Figure 10, which is a close-up photograph of the



Figure 9. Oblique Aerial Photograph
of Oasis Gabre Oun
(From Goudarzi, 1970,
p. 17).

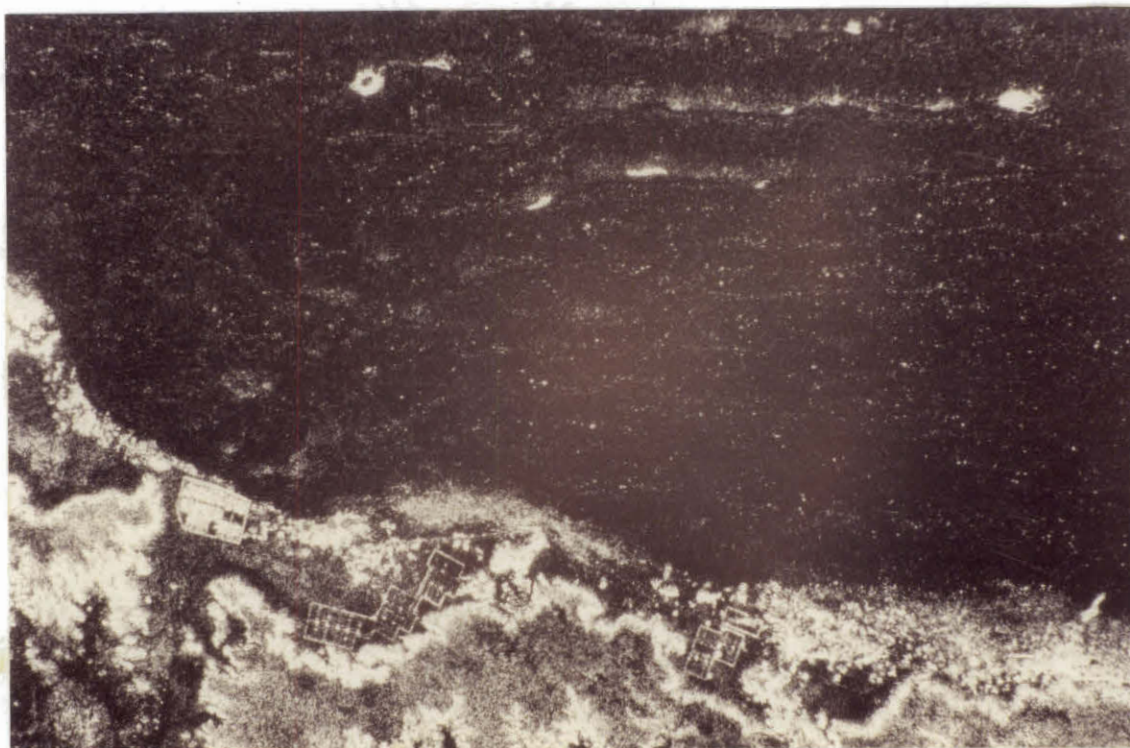


Figure 10. Close-up Photograph of SIR-A Image of the Messak
Escarpment, Wadi Agial and Oases (Gabre Oun in
upper right) in the Ubari Sand Sea (Plate 2,
M to P, 1 to 3).

east end of the SIR-A image in Plate 2. Several other oases display similar dual-terrain radar patterns, indicating lakes surrounded by palm trees. In addition to palm trees, crusts of salts, which occasionally form around some of the saline lakes, may produce a rough surface and thus a bright radar return.

Between the Ubari Sand Sea and the Messak escarpment lies Wadi Agial (I5 to P1). Numerous palm groves, towns and roads are visible on the radar imagery within Wadi Agial, which averages 7 km wide and parallels the entire length of the escarpment. The palm groves are imaged as clusters of bright spots along the central part of the wadi; towns are higher-density bright clusters, commonly within palm groves (Figure 10). Photographs in Klitzsch and Baird (1969, p. 69, 73 and 78), taken south of Germa, show palm groves near the center of Wadi Agial and sand dunes of the Ubari Sand Sea in the background.

The environment along Wadi Agial has long been hospitable to habitation as made evident by ancient ruins, foggaras, graves and rock drawings and carvings (Klitzsch and Baird, 1969; Daniels, 1969). Foggaras are ancient subsurface aqueducts. They were built by excavating aligned pits 5 to 10 m apart and then digging horizontal galleries between the bottoms of the pits to form a continuous duct. The foggaras generally are perpendicular to the Messak escarpment and slope into the center of Wadi Agial. Presumably they were built to tap Mesozoic sandstone

aquifers and/or underflow of the wadi alluvium. This network of foggaras probably irrigated extensive cultivations during the transition from a wet early Holocene climate to the current hyperarid climate. On the SIR-A image, between the Messak escarpment and Germa, are several faintly detectable lineaments, which may correspond to foggaras (K3). One oriented about N30W and 2 km long, which extends from the escarpment to a bright area mapped as Germa, may be the foggara that is well defined in a photograph in Klitzsch and Baird (1969, p. 78). A close-up surface photograph (Klitzsch and Baird, 1969, p. 73) of what appears to be the same foggara shows an average width of about 10 m with piles of excavated rubble as much as 2 m high. These dimensions should be large enough to be resolved in the SIR-A image, but the foggara is parallel to the look direction, the poorest orientation for its enhancement. Combined lengths of foggaras in the Germa area may be as much as 2000 km (Klitzsch and Baird, 1969, p. 73); however, there is little evidence of this in the SIR-A imagery. Perhaps radar imagery of higher resolution and larger scale would define the foggaras better.

One of the most evident cultural features in Wadi Agial are large, square to rectangular gridded networks. The largest is a short distance west of the town of Ubari (I5); others are at M2, N2 and O1, which are shown best in Figure 10. The large dimensions (5 X 8 km at Ubari) and highly organized grids indicate that these networks may be

evaporation ponds built to exploit deposits of potash and other valuable salts which exist along Wadi Agial.

Evaporation tests were performed at one salt deposit in a depression along the south-central margin of the Gargaf in which networks of 3 m square pits were dug to the water table and brines accumulated and evaporated (Goudarzi 1970, p. 83-88). Successful results may have prompted exploitation of the salt deposits along Wadi Agial.

Differentiation of Terrain by Radar

Signature

Four distinct types of terrain are in this segment of radar imagery (Plate 2). Wadi Agial is dominated by cultural features; its radar signature varies from dark, over bare alluvium, to bright, over palm groves and towns.

The Ubari Sand Sea generally is smooth; consequently its radar image is very dark. Slopes of linear sand dunes that face the look direction return a moderate amount of radar energy. The surface roughness of palm groves, and perhaps of salt crusts in oases are the origin of bright spots within the sand sea.

The rocky surface of Hamada Murzuk is imaged brightly and contrasts sharply with the black image of the smooth sarir to the south. Sarirs and hamadas are common throughout the Central Sahara. The unique ability of radar to detect surface roughness easily distinguishes these two types of surfaces.

Ghat Segment, Libya and Algeria

The Ghat segment (Plate 3) covers a large variety of terrain; it spans from the eastern edge of the Hoggar Massif near Djanet, Algeria across the western flank of the Murzuk basin in Libya. Cambro-Ordovician sandstones of the Gargaf Group and the Silurian-Devonian sandstones of the Acacus Mountains form two distinct, broaduestas, strata of which dip eastward into the Murzuk basin. The regional setting is displayed well in the two Gemini XI hand-held LFC oblique photographs (Plates 2 and 3), which were useful ancillary data in the interpretation of this segment of radar imagery.

At the far southwestern edge of the segment (B1 to A5) Erg D'Admer covers probable basement complex. The very low radar return produced a nearly black image in this sand-covered area, indicating a very smooth surface that reflected most radar energy away from the antenna. A small segment of basement complex is exposed near Djanet (D4). Deep weathering of highly fractured basement rocks has produced rough terrain, which returns much backscatter. Due to the relatively bright background return, the town of Djanet, the Djanet airport and other cultural features could not be reliably located in this portion of the radar image. Near the southwestern boundary of terrain where basement rocks crop out very bright ridges are surrounded by a nearly black image (D1 to C3). Here, the Gemini photograph in Plate 2 confirms that ridges of basement rock were left high-standing by differential erosion; they protrude above

the smooth sand-covered fringe of Erg D'Admer, producing the highest contrast of radar return detectable on the entire image strip.

Although difficult to distinguish from basement rock on the SIR-A image, Cambro-Ordovician sandstone crops out in a small area west of Djanet, where it is highly dissected and partially sand-covered (B4-B5). A north-northwest-trending escarpment is on the eastern side of the basement complex, along the contact between basement rocks and the resistant Gargaf Group sandstones (D1 to D5). Elevation of the margin of the escarpment is "consistent" at 1800-1900 m (elevations from DMA map nos. ONC H-3 and TPC H-3D). Highlands above the escarpment are known as the Tassili N'Ajjer, which rims the northeastern margin of the Hoggar Massif. In the Ghat segment Cambro-Ordovician sandstones form a 55-km-wide cuesta beneath which strata dip eastward. At the eastern contact with the Silurian Tanezzuft Shale, elevation of the margin of the cuesta averages about 800 m (H1 to J5). A north-trending 10-km-wide strike valley has formed along the outcrop of the Tanezzuft Shale. Portions of the Tanezzuft are sand-covered -- especially along Wadi Tanezzuft which trends along the Gargaf-Tanezzuft contact; consequently the radar image is dark. At the north end of the valley the triangular shaped town of Ghat (J4) can be recognized easily, due to its high contrast (bright return) against the smooth, partially sand-covered terrain of the Tanezzuft Shale. The Ghat area is shown in detail in the close-up

photograph of SIR-A imagery in Figure 11. The runway of the Ghat airport is barely visible a short distance east of Ghat. The towns of Fehouet and Al Barkat are also detectable, along with connecting roadways. These three ancient towns were colonized around oases that are fed by eleven springs, six of which are at Ghat (Burdon, 1980). The radar signatures of the towns are bright due to buildings, palm trees and stone walls.

Along the eastern border of the Tanezzuft valley a prominent escarpment is formed by the Silurian Acacus

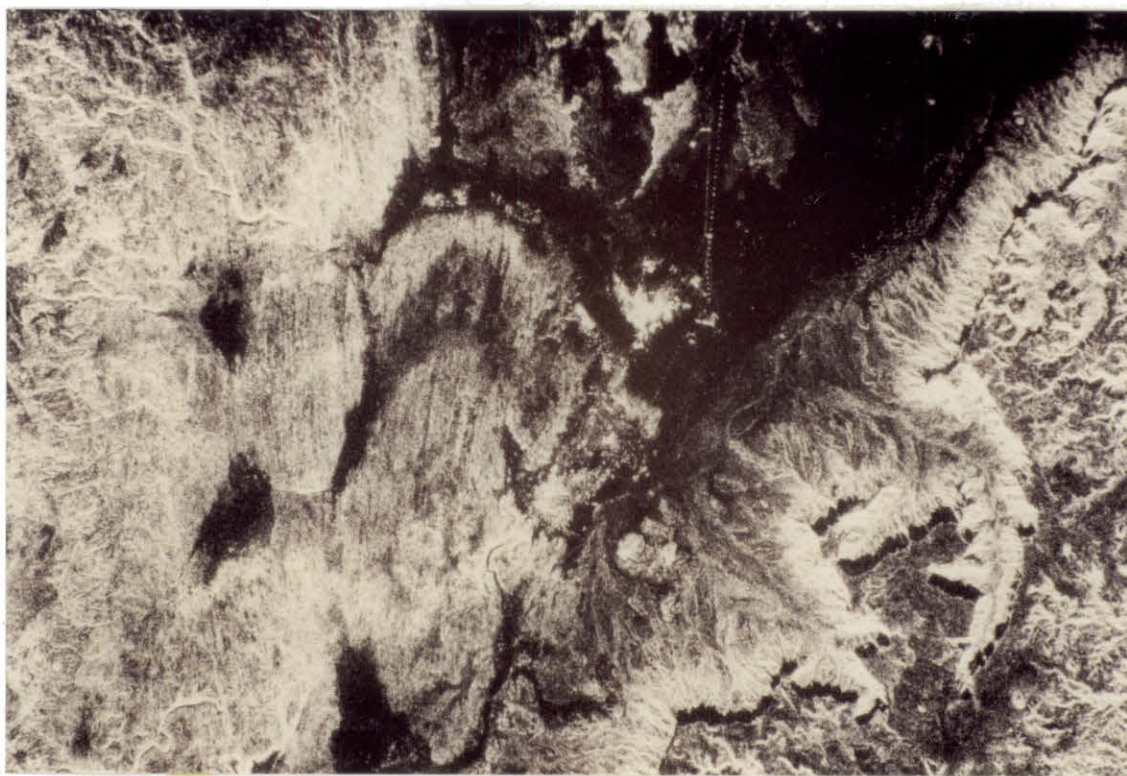


Figure 11. Close-up Photograph of SIR-A Image of Ghat and Surrounding Area (Plate 3, H to K, 3 to 5).

Sandstone (I1 to K5). Long shadows along slopes that faced away from the north-northwest look direction indicate substantial relief of the escarpment (Figure 11; Plate 3). DMA map TPC H-3D indicates approximately 450 m of local relief. Bright returns along non-shadowed slopes indicate rough surfaces, perhaps of landslides and colluvium.

The Silurian Acacus Sandstone and the Devonian Tadrart Sandstone, form the Acacus Mountains, the second broad cuesta east of the Hoggar Massif (Plates 1 and 3). On the average this cuesta is 45 km wide; strata dip eastward into the Murzuk basin. Position of the Acacus-Tadrart contact is unclear. Although the Caledonian unconformity is between the two sandstones (Figure 8), their lithologies are similar (Bellini and Massa, 1980; Klitzsch, 1969). A subtle east-west change in the general character of the image approximately at the central portion of the mountains (K1 to M5), may be related to the Acacus-Tadrart contact.

The eastern boundary of the Acacus Mountains is defined clearly in the image (N1 to N5); probably it corresponds to the Devonian Tadrart Sandstone - Devonian Kasa Shale contact. As interpreted, the rough Tadrart terrain produces a bright image, whereas the Kasa Shale and overlying shale and interbedded sandstones of the Carboniferous Mrar Formation underlie relatively smooth terrain and consequently produced a dark radar image. Additionally, much of the Mrar is covered by smooth sands of Iguidi Ouan Kasa (O1 to P5).

Comparison of SIR-A with Gemini XI

Photographs

The Gemini photographs are oblique, and of smaller scale and lower resolution than the SIR-A imagery. They show much less detail than the radar imagery; however some reliable general comparisons can be made. Sand-covered areas on the Gemini colored photographs are light-toned, whereas basement and sandstone terrains are dark; this is the reverse of SIR-A image brightness. Light-colored, sand-covered drainage valleys through the Acacus Mountains contrast sharply against dark highlands in the Gemini photographs, whereas on SIR-A imagery the "smooth" valley floors are dark, with bright walls and highlands. The best example of this is Oued Teshuinat which is clearly visible in the Gemini photographs and SIR-A (J1 to M1).

Cultural features, such as towns and roadways, were not distinguishable on the Gemini photographs. This was at least partly due to the lower resolution of the photographs, but may also be due to the low color contrast between mud buildings on sand-covered wadis. The roughness contrast between towns and wadis is high, which is optimal for distinction by radar.

On Gemini photographs basement terrain appears to be more similar to Acacus-Tadrart sandstone terrain than to Cambro-Ordovician terrain, whereas the basement is more similar and even locally difficult to distinguish from Cambro-Ordovician terrain in SIR-A imagery. In the area

west of Djanet (C4, C5), this contrast on Gemini photographs helped to distinguish the Cambro-Ordovician sandstones from basement rocks. Cambro-Ordovician sandstones appear smoother than Acacus-Tadrart sandstones in the Gemini photographs, which correlates well with the radar image.

Differentiation of Terrain by Radar

Signature

Terrain of the Gargaf Cambro-Ordovician sandstones of the Tassili N'Ajjer is of appearance substantially different from terrain of the Acacus-Tadrart sandstones. The Gargaf terrain is dominated by lineaments as long as about 34 km. The fracture-controlled stream-drainage pattern in the western half of the Gargaf outcrop is linear, whereas drainage in the eastern half is dendritic, with several meandering stream courses. The fracture density decreases to the east, away from the basement complex. Topographic slope is very consistent and eastward across the entire Gargaf outcrop (DMA map no. TPC H-3D). The change in drainage pattern eastward may reflect proximity to and distance from basement.

Stream dissection of the Gargaf appears relatively shallow. Burdon (1980) reported that the Ordovician sandstone near Ghat is tightly cemented quartzite, on which he observed numerous standing pools of water. He also observed joints that generally were tightly cemented, although he suggested that the oases of Ghat, Al Barkat and

Fehouet are fed through open joints over domes or folds (Burdon, 1980, p. 598). From a study of subsurface fluid pressures, Chiarelli (1978, p. 681) concluded that there is little or no surface infiltration at outcrops of Cambro-Ordovician sandstone in the Tassili N'Ajjer. These observations support the general conclusion, from interpretation of SIR-A imagery, that the Cambro-Ordovician sandstones are very resistant to erosion and highly susceptible to fracturing, indicating they are tightly cemented and brittle.

The radar return from sandstones of the Gargaf Group is brighter than might be expected from resistant, relatively little-dissected terrain. Photographs of the Gargaf near Djanet (Massa et al., 1972, p. 497, 503, 504) show medium bedded sandstones with abundant, nearly vertical fractures. The combination of medium bedding and fracturing has produced a broken, blocky, locally stair-step terrain with a rough surface; this would produce a bright radar image.

In contrast, the Acacus-Tadrart sandstone terrain is highly dissected by deep valleys arranged in dendritic patterns. Few lineaments were observed, although several well defined ones are along the eastern margin (N1-N2); these are similar in appearance and setting to ridges of basement rock above Erg D'Admer. The image brightness of Acacus-Tadrart terrain is approximately equal to that of Gargaf terrain, although the surface roughness correlated with image brightness is controlled by deep drainage

dissection rather than by bedding and fracturing.

Although terrain of basement rock covers a relatively small area and is partially sand covered, it is distinct from the other terrains. There appears to be two general rock types composing the basement complex. Granitic rocks are highly fractured and deeply weathered, which produced a very bright radar image (D4), whereas metamorphic rocks are banded and less fractured (D1 to C3).

The fourth type of terrain is the smooth terrain of shale outcrop and sand-covered areas. Erg D'Admer, Wadi Tanezzuft and Iguidi Ouan Kasa are within this category of terrain. Their smooth, low-relief surfaces backscatter little radar energy, producing dark gray to black images.

Fracture Patterns

Plate 3 shows a rose diagram with the same orientation as the SIR-A image. There were 21 well-defined lineaments longer than 2.5 km measured from the SIR-A image within Cambro-Ordovician sandstones in the western Tassili N'Ajjer. The dominant strike is N63W. Two minor trends are N5W and N48E. The longest continuously mapped lineament is about 34 km (E4 to F2), and lengths of 10 to 15 km are common. Evidence of lateral displacement was not detected. The lineaments almost certainly are evidence of post-Ordovician (Caledonian and/or Hercynian) fracturing and faulting of basement.

Massa et al. (1972) studied fractures in the Cambro-

Ordovician sandstones near Djanet and several other areas along the Tassili N'Ajjer, in an attempt to better understand oil production from correlative sandstones in the Hassi Messaoud field to the north. Fault displacements and slickensides are observable in some of their photographs of the highly fractured Cambro-Ordovician sandstones east of Djanet. In this area they measured regional fracture trends of N9E and N60W (Massa et al., 1972, p. 513).

Fracture trends in the basement complex near Djanet generally correspond to the trends in Cambro-Ordovician sandstones. Several lineaments even appear to be continuous across the basement rock-sandstone contact (D3 to D5).

About 5 km west of Ghat, closely spaced lineaments, averaging 15 km long, are in Cambro-Ordovician sandstone (Plate 3, I3-I4; Figure 11). The arrangement of these lineaments appears much different from those in the upper elevations of the Tassili N'Ajjer. They probably are sets of closely spaced joints, possibly enhanced by wind-erosion. There are two distinct orientations: N40W and N25W.

Although very few lineaments can be seen in the Acacus Mountains, several north-trending lineaments within the Tadrart Sandstone may be fractures translated from the basement.

Tiririne Segment, Algeria

The Tiririne segment (Plate 4) of radar imagery straddles the Central and Eastern belts of the Hoggar Massif (Plate 1; Figure 7). The metamorphic basement rocks are

highly folded and faulted, and intruded by granitic plutons, forming an extremely complex terrain; most elevations are between 900 and 1300 m. Stream drainage is generally eastward and seems to have been superposed.

A partial (approximately 110 km X 110 km) Landsat Thematic Mapper scene covers a large portion of this SIR-A image segment; it was very useful in the interpretation. Its 30-m resolution and color generally show more detail than the SIR-A image (40-m resolution). The Landsat scene was processed on a 486 IBM-compatible personal computer. Color photographs shown here were taken directly of the computer monitor using a tripod-mounted camera, a shutter speed of 1 second and telephoto F-stops of 8 to 11. Scenes are composed of bands 7 (assigned to red), 5 (assigned to green) and 2 (assigned to blue), resulting in a false-color image with fairly good color balance and contrast. Plate 4 contains the partial Landsat scene (1 cm = approx. 12 km); photographs within the text are of subsets of that scene and show greater detail. North is toward the top in all photographs of Landsat imagery presented here.

The Tiririne SIR-A segment reveals at least three major north-northeast-trending faults. These three faults are shown in Figure 12, a detailed subset of the southwestern quarter of the Landsat scene (Plate 4, left). The most significant fault strikes N15E (Plate 4, B1 to H5). This fault zone is as much as 2 km wide and separates two distinct terrains. To the east are granitic rocks through



Figure 12. Subset of Southwest Quarter of Landsat Scene, Tiririne Segment, Algeria (1 cm = approx. 6 km).

which two lesser faults (D1 to K5 and E1 to K5) converge to the north; these faults have been described as mylonitic, and one sample near their junction was dated at 553 m.y., indicating late Pan-African or post-Pan-African emplacement (Bertrand et al., 1978, p. 364). Numerous dikes, averaging about 3 km long, are within the granites. To the west high-relief, bedded metamorphic rocks contain well defined antiforms and synforms in the area C2 to E5. Along the western margin of the metamorphic rocks is a 5-km-wide, low relief linear zone (B1 to D5) mapped as a schist belt by Bertrand et al. (1986, p. 956). Another schist belt (F4-F5)

bounds the eastern margin of the folded metamorphic rocks.

The schist belts, and folds within the metamorphic rocks, generally strike about N10W, forming an angle of about 25 degrees to the bounding fault zone, indicating that the fault (B1 to H5) may be a right-lateral strike-slip fault. Bertrand et al. (1986, p. 963) show this fault as a right-lateral strike-slip fault, which evolved from a thrust fault (thrust to east) and likely originated prior to the Pan-African orogeny. The two lesser faults to the east, also mapped as right-lateral faults by Bertrand et al. (1978, p. 353), are younger -- late Pan-African to post-Pan-African, as indicated by the dated sample from the granite through which they trend.

In the eastern half of the SIR-A image, metamorphic rocks have been intruded by subcircular granitic plutons (J2, K4 and L4). Terrain in this part of the image is partially sand-covered and generally of low relief. The contact (J1 to M5) between the metamorphic rocks in the east and granitic rocks in the west forms the boundary between the Eastern and Central Hoggar belts. Metamorphic rocks in this portion of the Eastern belt are composed mostly of the volcano-clastic Tiririne Formation, as much as 8000 m thick, and considered by Bertrand et al. (1978, p. 371) to have been deposited in a subduction trough along the western margin of the Eastern Hoggar belt between 660 and 725 m.y. ago. Much of the tectonic fabric visible in this SIR-A image may have resulted from continental collision during

the Pan-African orogeny.

Sand and/or fluvial deposits cover a broad valley along the eastern margin of the image (O1 to N5). Outliers of Cambro-Ordovician sandstone are along the edges of the valley. A geologic map by Bertrand et al. (1978, p. 353) covers the eastern half of this segment of SIR-A imagery; it was very useful in the interpretation.

Comparison of SIR-A with Landsat Imagery

As with the Gemini XI photographs, there is generally an inverse relationship of brightness between the radar and Landsat image. Bright areas in the Landsat image are generally due to high reflection from sand, whereas the sand-covered areas appear dark in the radar image; the sand reflects most backscatter away from the antenna. Bright areas in the radar image generally correspond to high relief features which return much backscatter. High relief areas in the Landsat imagery are free of sand and thus darker, and may be partly in shadow.

The illumination direction of the radar image is from the southeast (N145E), whereas it is from the east (N88E) in the Landsat image. Although the illumination directions are about 57 degrees apart, they are from the same general direction, resulting in high-relief features being shadowed similarly in both images. This can be seen clearly in the close-up photograph (Figure 13) of section C2 of the SIR-A image in Plate 4, and the corresponding Landsat subset

(Figure 14). High-relief east-facing slopes are illuminated and west-facing slopes are in shadow on both images (north is toward the top in all photographs of imagery in text). The sun illuminated the Landsat scene from 59 degrees above the horizon, whereas the SIR-A image was illuminated by the radar beam from about 47 degrees (look angle) above the horizon.

The major right-lateral strike-slip fault (B1 to D3) strikes north-northeast through the centers of the images (Figures 13 and 14). To the west, what appears to be a doubly-plunging antiform is visible. The schist belt is in the southwestern corner. Granitic rocks outcrop to the east of the fault. Sand covered areas are bright in the Landsat image, but dark in the radar image. Several dikes within granitic terrain extend slightly above sand and are imaged brightly by SIR-A (Figure 13), but as very faint dark streaks in the Landsat image (Figure 14).

Another comparison is made northward along the same fault zone (E3). The granitic terrain, crossed by dikes, is in the southeastern parts of the images (Figures 15 and 16). Against the western edge of the fault zone, in the bottom center of the images, is a north-trending doubly-plunging antiform, about 2.5 km wide. Along the western boundary of the antiform is a very narrow synform, about 400 m wide. Another antiform may be immediately to the west of the synform. A plunging nose of this antiform is to the north. Along the western edges of the images, another

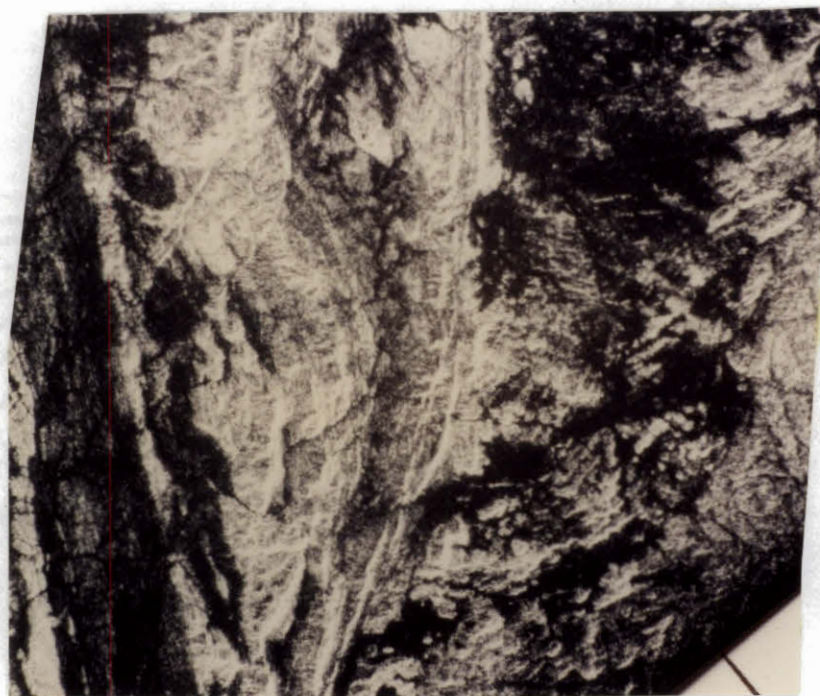


Figure 13. Close-up Photograph of
SIR-A, Plate 4, C2.



Figure 14. Landsat Subset of Figure 13
(1 cm = approx. 2.6 km).

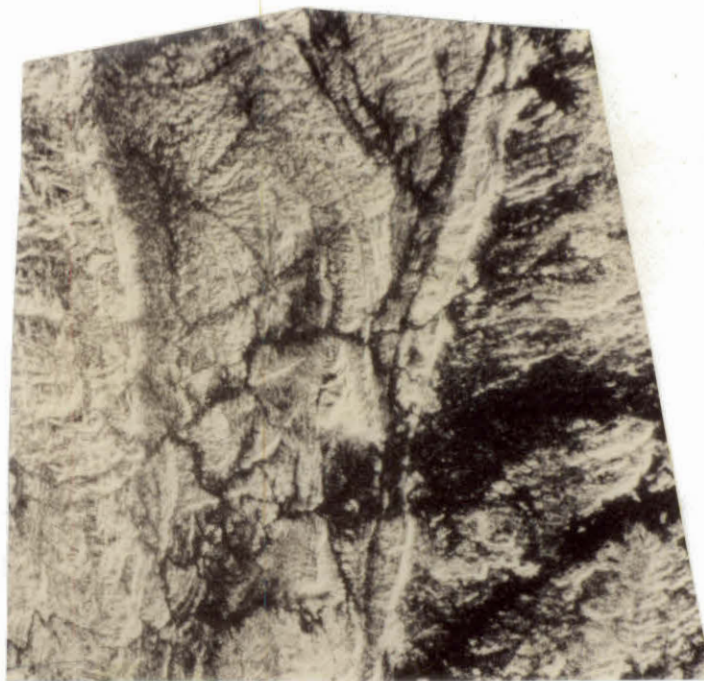


Figure 15. Close-up Photograph of
SIR-A, Plate 4, E3.

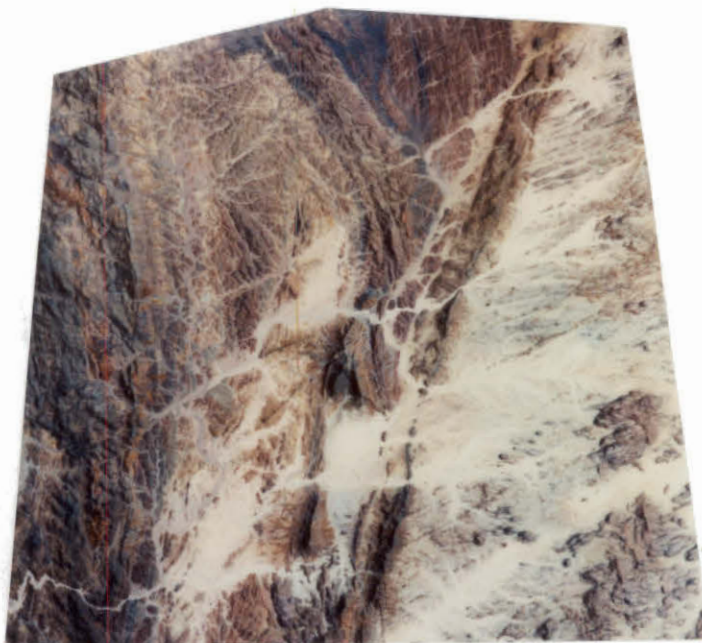


Figure 16. Landsat Subset of Figure 15
(1 cm = approx. 3 km).

north-trending fold is detectable; it appears to be a south-plunging antiform (see Plate 4 for positions of fold axes). Bedding, which is so well defined in the western antiform and the folds to the east, is not apparent in the rocks in between, indicating that these may be high-grade metamorphic (gneiss or granulite) or granitic rocks (Plate 4). These rocks are bounded on the west and east by bedded metamorphic rocks, then by schist belts, giving the general appearance of a massive anticlinorium which may have been formed due to right-lateral strike-slip fault displacement (see also Plate 4 and Figure 12).

The two mylonitic right-lateral strike-slip faults within granitic terrain (G2-H3) are imaged by radar (Figure 17) and Landsat (Figure 18). Numerous dikes are in this area, most of which are partially covered by sand. They are difficult to locate in the Landsat image, except where completely exposed, they appear as dark streaks. The dikes generally are much more visible in the radar image. Even though they are covered by sand, they still have some relief which is manifest as bright streaks on the radar image. There may also have been some penetration of the radar beam into the sand, the beam having been strongly reflected from the buried dikes. Three dikes (Plate 4, H3) in the northeastern corners of the images are brightly imaged in radar, but only faintly visible in the Landsat image.

Two circular features (K3-K4 and L4) are compared in a SIR-A image (Figure 19) and a Landsat subset (Figure 20).

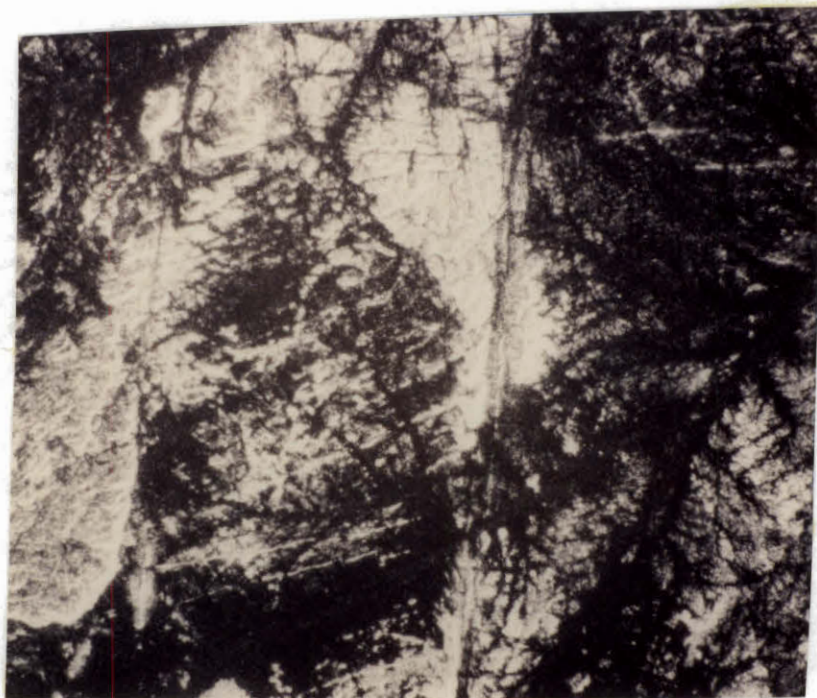


Figure 17. Close-up Photograph of
SIR-A, Plate 4, G3.



Figure 18. Landsat Subset of Figure 17
(1 cm = approx. 2.7 km).

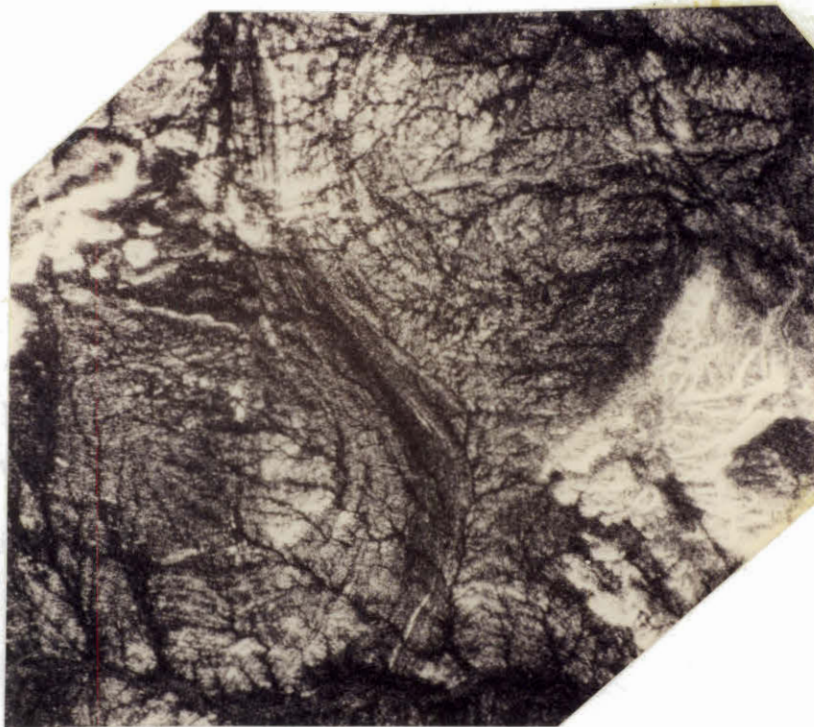


Figure 19. Close-up Photograph of
SIR-A, Plate 4, K4.

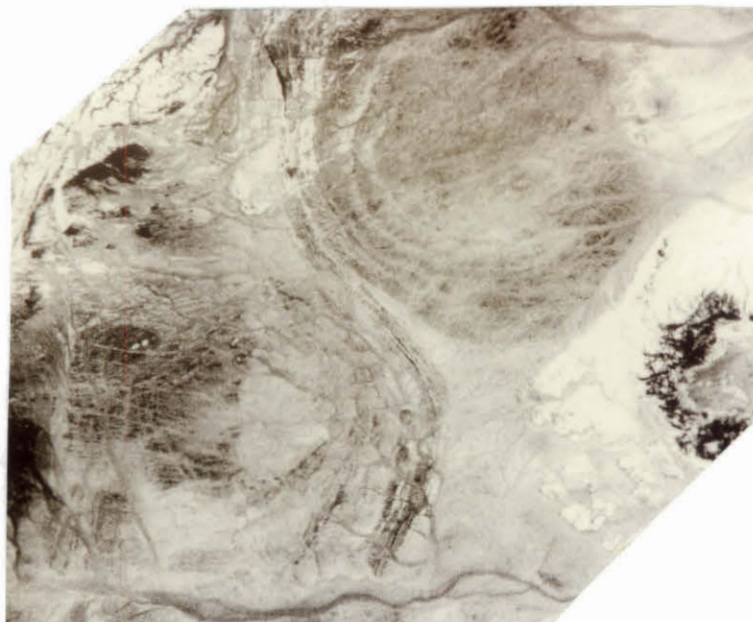


Figure 20. Landsat Subset of Figure 19
(1 cm = approx. 3 km).

The Landsat image is a ratio of band 7 to band 4. The lighter areas correspond to stronger reflection in band 7, whereas dark areas appear where reflection in band 4 is stronger. The circular feature to the northeast (Figure 20), which is defined so well in the ratio image, is also shown in the northwestern quarter of the 3-band composite image in Figure 21, in which it appears to be mostly sand-covered and featureless. This comparison illustrates the major advantage of Landsat imagery over radar imagery: The large digital data set of seven distinct bands can be combined and enhanced in a very large number of ways. The radar image defines the circular features nearly as well as the Landsat image, although definition of some drainage patterns and linear features is better in the radar image.

The northeastern circular feature is the Adaf granitic pluton. Several samples from its southern third were dated 585 and 604 m.y., indicating it was emplaced during the Pan-African orogeny. The Adaf pluton, about 13 km in diameter, has been described as being concentrically layered by different foliated and nonfoliated rock types, ranging from granite to dark adamellite and hornblende granodiorite, to sheets of gneiss; foliations dip inward (Bertrand et al., 1978, p. 370). The southwestern circular feature is similar to the Adaf pluton, but contains more metamorphic rocks along its southeastern margin, which are apparent in the SIR-A and Landsat imagery. The intimate layering of metamorphic and granitic rocks around these circular plutons



Figure 21. Landsat Subset of "Crypto-Volcanic" Feature in Plate 4, L3 (Note Frame of Computer Monitor; 1 cm = approx. 3 km).

imparts a distinctive annular, banded structure visible in the radar and Landsat images.

Differentiation of Terrain by Radar

Signature

Two general categories of rock types, granitic and metamorphic, are distinguishable in the Tiririne SIR-A segment of the Hoggar Massif. In most cases, each type can be distinguished by its radar signature. Granitic terrain can be identified in two general settings: As fractured,

high-relief masses (D1, F1, F3), and as eroded, low-relief, partially sand-covered plutons (J2), commonly with numerous bright streaks representing dikes (G4, D2). Dikes may be present in high-relief terrain (Figure 18), but are not apparent in the radar imagery due their low roughness contrast in granitic masses.

Metamorphic rocks are distinguished by bedding or banded structure. Bedding is very apparent in the high-relief fold belt (C2 to E5) just west of the major right-lateral strike-slip fault (B1 to H5). In low-relief, partially sand-covered terrain, the banded structure of metamorphic rocks is visible at numerous places (A4, J1-K1, K3, L2). In most of the eastern half of the SIR-A image the slightly brighter, banded metamorphic terrain is readily distinguishable from slightly darker, low-relief, non-banded granitic terrain.

The two schist belts (B1 to D5, and F4 to F5) comprise a distinct metamorphic terrain. These belts are narrow and display strong lineation along their lengths. They are bounded by faults, at least on one side and perhaps on both. The belts are of relatively low relief; the belt from B1 to D5 forms a narrow valley longer than 50 km, which is the straightest, and one of the most distinct lineaments observed on the entire SIR-A image strip. Its closely spaced lineation is best defined in the southeastern corner of the Landsat subset (Figure 14), although lineation is also apparent in the radar image (Figure 13).

In some terrain the radar signature is ambiguous. The rocks between the junction of the two mylonitic fault zones (I4) show faint banded structure, indicating that they may be metamorphic, whereas their high relief and fractured appearance indicate granite. Bertrand et al. (1978, p. 353) mapped these rocks as granite. The banded structure of the rocks apparently is due to fracturing and/or minor faulting, which could be expected by consideration of the close proximity of the terrain to two large faults. In other areas, absence of banding may not preclude the presence of metamorphic rocks (G1-H1). In this area, Bertrand et al. (1978, p. 353) mapped metamorphic rocks where banded structure is not apparent. In some terrain, granites may be mixed with metamorphic rocks (Adaf pluton L4; I5-J5). In other cases, granite may not be distinguishable from high-grade metamorphic rocks in which bedding and banding may have been destroyed (E4).

One unusual high-relief feature is in the radar image at position L3. It is shown in detail on a Landsat subset (Figure 21). It is surrounded by folded metamorphosed rocks of the Tiririne Formation, and a portion of it is mapped as granite (Bertrand et al., 1978, p. 353). The landform is unusual in that the center is eroded and partly sand-covered, giving the general appearance of a volcano. Although late Tertiary volcanoes are in the Hoggar Massif to the west and north (Plate 1), they have not been reported in this area. The "crypto-volcanic" feature may be an igneous

intrusion, of which rock in the central part is less resistant than rock in the remainder of the pluton or sill; alternatively, it could be an astrobleme.

Cambro-Ordovician outliers near the eastern margin of the radar image are of medium brightness and appear featureless, attributes that distinguish them from other rock types. Sand and/or fluvial deposits between the outliers are dark in the radar image.

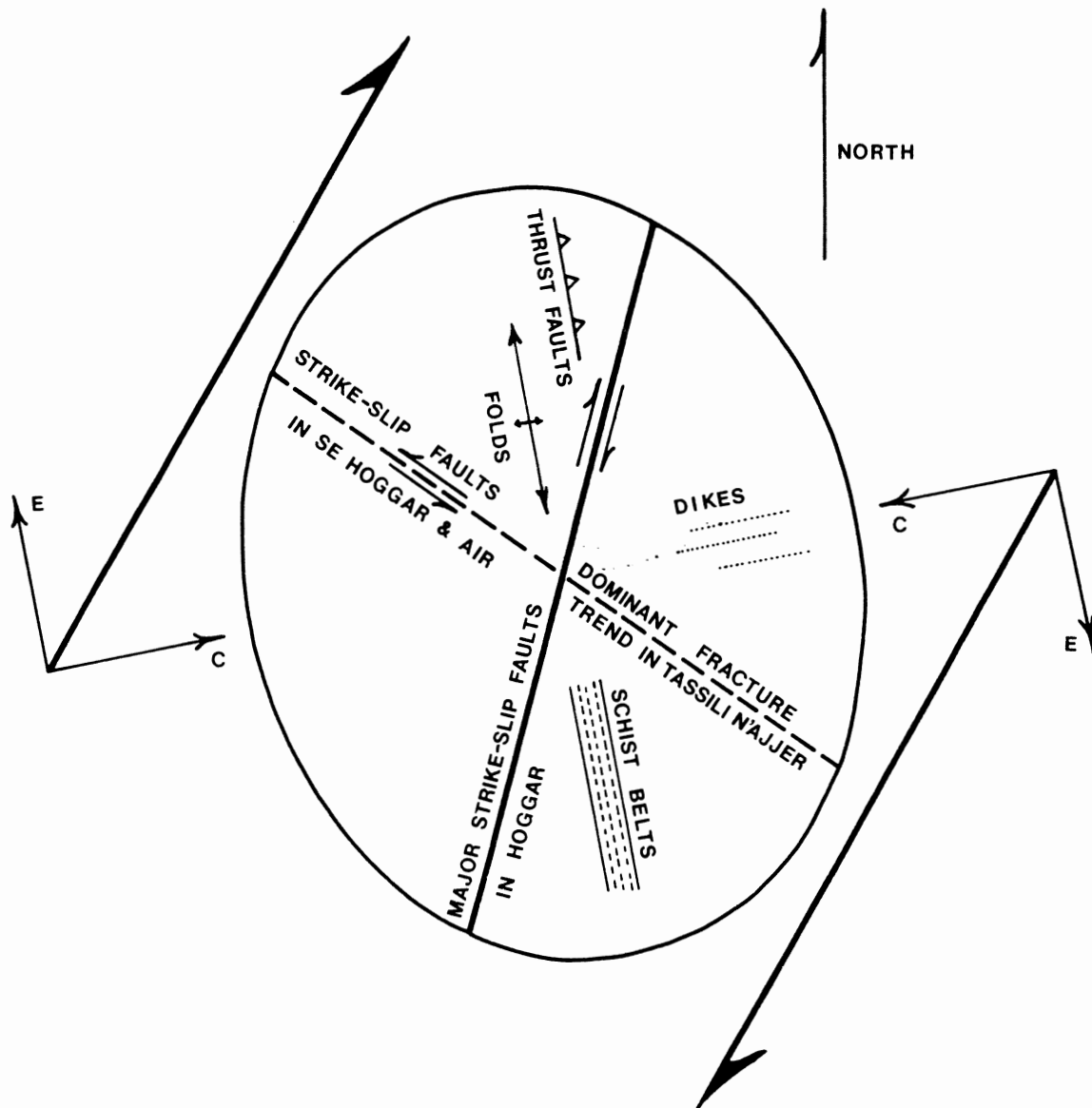
Pan-African Stress Regime Implied by Tectonic Elements

Fifteen major faults, fault zones and schist belts were observed on the SIR-A image strip across the Hoggar Massif and the Iforas extension. Most of these lineaments are faults; the dominant trend is about N10E. These faults are evident on the International Tectonic Map of Africa (Sheets 1 and 2), and Bertrand et al. (1986, p. 963 and 968; 1978, p. 353) indicate that many of the north-northeast-striking faults are right-lateral strike-slip faults. The major fault on the Tiririne segment of SIR-A (Plate 4, B1-H5) strikes N15E and is bounded on the west by folds with an average trend of N10W, which provide evidence of right-lateral strike-slip displacement. Other north-northwest trending folds, considered to have been formed by the Pan-African orogeny, are known in the Hoggar (Bertrand and Lasserre, 1976, p. 356). The fault in section G5 of Plate 4, and other north-northwest-striking faults in the Hoggar

Massif, are mapped by Bertrand et al. (1986, p. 956) as thrust faults.

Faults and folds were produced or rejuvenated during the Pan-African orogeny, the last major orogeny to widely and profoundly affect the basement rocks of the Central Sahara. A working hypothesis of the Pan-African stress regime in the Hoggar Massif can be formed: The compressional stress component trended N75E, perpendicular to the folds, and the extensional stress component trended N15W, parallel to folds (Figure 22). The compressional and extensional stress components were both in the horizontal plane and resulted from northeast-southwest wrenching, which may have been caused by oblique, convergent continental collision. The intermediate stress component was vertical. This stress regime would tend to produce right-lateral strike-slip faults striking north-northeastward, and complementary left-lateral strike-slip faults striking northwestward (Harding, 1974; Wilcox et al., 1973).

Several additional tectonic elements support this proposed explanation of the stress regime. Dikes mapped on the Tiririne segment of SIR-A (Plate 4) strike mostly east-northeast. The dominant strike is N75E, exactly perpendicular to the trend of the proposed extensional stress component. Late fluids of granitic intrusions would tend to fill extensional fractures or faults. Numerous dikes and extensional joints, both trending east-northeast, have been reported in the Air Massif of northern Niger



STRESS COMPONENTS
DERIVED FROM WRENCHING:

C - COMPRESSION
E - EXTENSION

Figure 22. Plan View of Hypothesized Pan-African Stress Regime in Southern Algeria and Northern Niger, with Tectonic Elements Observed in the Hoggar and Air Massifs (Adapted from Harding, 1974, p. 1291).

(Black and Girod, 1970, p. 198).

Although generally sparse, there are northwest-striking faults in the Hoggar Massif, some of which have been indicated by Bertrand et al. (1986, p. 963, 968) as left-lateral strike-slip faults. Northwest-striking faults are more common in southeastern Hoggar, most of which appear to displace granitic intrusions in a left-lateral sense (International Tectonic Map of Africa, Sheet 2). Numerous northwest-striking left-lateral strike-slip faults, along with several complementary north-northeast-striking right-lateral faults, are well documented in the Air Massif (Black and Girod, 1970, p. 190, 198). Left-lateral strike-slip faults in the Air and Hoggar are antithetic to the right-lateral strike-slip faults, and fit well into the proposed stress regime (Figure 22).

Schist belts on the Tiririne segment of SIR-A trend parallel to the extensional stress component. Although the genesis of these belts is not well understood, it seems likely that they would form parallel to extension and perpendicular to compression.

Some investigators have considered the major north-northeast-striking faults of the Hoggar Massif as having originated as thrust faults, but rejuvenated during the Pan-African orogeny as right-lateral strike-slip faults (Bertrand et al., 1986, p. 962). This could be explained by rotation of the stress regime, caused by a change in the direction and angle of crustal convergence. North-trending

thrust faults would have tended to form during head-on east-west continental convergence, during which wrenching would have been absent and the extensional stress component would have been vertical. During transition to northeast-southwest oblique convergence, wrenching would have been introduced, the extensional stress component would have rotated to the horizontal and strike-slip movement would predominate. This rotation of the stress field has been proposed for the Air Massif, but has been attributed to erosion and isostatic readjustment of thickened crust (Black and Girod, 1970, p. 190).

Oblique convergence would tend to produce at least a small amount of thrust displacement along the right-lateral strike-slip faults, and small amounts of strike-slip displacement may have occurred along the original pre-Pan-African thrust faults if initial convergence was not exactly head-on. Some of the major north-northeast-trending faults may not have been purely thrust or strike-slip faults, but rather better described as dominantly thrust or dominantly strike-slip faults. Two distinct directions and types of crustal convergence may not be necessary to explain the fact that many of the north-northeast-striking faults in the Hoggar have both thrust and strike-slip displacement. A single, northeast-southwest oblique crustal collision could have produced thrust and strike-slip movement along the same fault at the same time, with associated folds and dikes.

CHAPTER V

CONCLUSIONS

1. The SIR-A radar imagery contained a large amount of information, which allowed efficient reconnaissance of portions of the vast Central Sahara.

2. Six categories of terrain were distinguished by their radar signature over the approximately 30,000 sq km examined (Table II).

TABLE II

CENTRAL SAHARAN TERRAINS DISTINGUISHED BY RADAR SIGNATURE

<u>TERRAIN</u>	<u>RADAR RETURN</u>	<u>CHARACTERISTICS</u>
Sandstone	Bright	Fractured (Tassili N'Ajjer), Dissected (Acacus Mountains), Rocky (Hamada Murzuk),
Wadi	Medium Bright to dark	Featureless (Tiririne outliers) Palm trees, cultural features
Sand Seas	Dark	Linear sand dunes, bright oases
Sarir	Dark	Featureless
Granite	Bright	High relief, massive, fractured
Granite	Medium	Low relief, drainage patterns
Metamorphic	Bright	High relief, bedded, folded
Metamorphic	Medium	Low relief, banded structure
Metamorphic	Medium	Low relief, linear (schist belts)
Metamorphic and/or Granitic	Medium	Annular banding (Adaf pluton), Lack of banding (gneiss or granite)

3. Ancillary conventional imagery greatly aided interpretation of the radar imagery; conventional imagery should be used whenever possible.

4. The SIR-A imagery showed much more detail than the two smaller scale, lower resolution Gemini XI photographs, although the regional setting was well displayed in the Gemini imagery.

5. SIR-A imagery compared well with Landsat Thematic Mapper imagery. The Landsat scene generally showed more detail, but in some cases the radar imagery showed better detail. Used together, they were a powerful tool for regional geologic mapping.

6. Radar imagery is limited in several respects:

- a. Inability to distinguish color.
- b. Scale distortion makes comparison with maps and other imagery difficult.
- c. Look direction overemphasises some features, while diminishing or hiding others.

7. Distinct advantages of radar imagery over conventional photographic or scanner imagery include:

- a. Ability of the mapper to distinguished smooth from rough microrelief.
- b. Contrast of some features is greater in radar imagery.
- c. Penetration of thin layers of dry sand, revealing buried features.

8. Maps, publications and photographs of surface

terrain were very useful and allowed verification of some interpretations.

9. SIR-A and Landsat imagery of the Tiririne area in the Hoggar Massif defined folds, faults and dikes, which supported the hypothesis that a Pan-African wrench stress regime existed, possibly caused by oblique crustal convergence, in which the compressional stress component trended N75E, the extensional stress component trended N15W and the intermediate stress component was vertical.

10. Surface mapping and/or large-scale aerial photographs will be required to answer questions raised during the interpretation: Are the gridded networks in Wadi Agial evaporation ponds? Where is the contact between the Acacus and Tadrart Sandstones? What are the rock types and structural relationships of the fold belt (Plate 4, C1 to E5) bounded by schist belts? What is the nature of the high-relief "crypto-volcanic" structure north of Tiririne (Plate 4, L3)?

SELECTED BIBLIOGRAPHY

- Allegre, C. J. and R. Caby, 1972, Chronologie absolue du l'Ahaggar occidental: Comptes Rendus Acad. Sc. Paris, Ser. D, v. 275, p. 2095-2098.
- Baird, D. W., 1969, Geological bibliography of the Murzuk basin region, in Geology, Archaeology and Prehistory of the Southwestern Fezzan, Libya: Petrol. Explor. Soc. of Libya, p. 139-150.
- Bankwitz, P. et al., 1968, Prakambrium: Verlag, Stuttgart, Germany, 702 p.
- Bellini, E. and D. Massa, 1980, A stratigraphic contribution to the Palaeozoic of the southern basins of Libya, in The Geology of Libya: Academic Press, New York, NY, v. 1, p. 3-56.
- Bertrand, J. M. L. and M. Lasserre, 1976, Pan-African and pre-Pan-African history of the Hoggar (Algerian Sahara) in the light of new geochronological data from the Aleksod area: Precambrian Research, v. 3, p. 343-362.
- Bertrand, J. M. L. and R. Caby, 1978, Geodynamic evolution of the Pan-African orogenic belt: A new interpretation of the Hoggar shield (Algerian Sahara): Geologische Rundschau, v. 67, p. 357-388.
- Bertrand, J. M. L., R. Caby, J. Ducrot, J. Lancelot, A. Moussine-Pouchkine and A. Saadallah, 1978, The late Pan-African intracontinental linear fold belt of the eastern Hoggar (Central Sahara, Algeria): Geology, structural development, U/Pb geochronology, tectonic implications for the Hoggar Shield: Precambrian Research, v. 7, p. 349-376.
- Bertrand, J. M., A. Michard, A. M. Boullier and D. Dautel, 1986, Structure and U/Pb geochronology of central Hoggar (Algeria): A reappraisal of its Pan-African evolution: Tectonics, v. 5, p. 955-972.
- Beuf, S., B. Biju-Duval, J. Stevaux and G. Kulbicki, 1969, Extent of "Silurian" glaciation in the Sahara: its influences and consequences upon sedimentation, in Geology, Archaeology and Prehistory of the Southwestern Fezzan, Libya: Petrol. Explor. Soc. of Libya,

p. 103-116.

- Black, R. and M. Girod, 1970, Late Palaeozoic to Recent igneous activity in West Africa and its relationship to basement structure, in African Magmatism and Tectonics: Oliver and Boyd, Edinburgh, p. 185-210.
- Black, R., R. Caby, A. Moussine-Pouchkine, R. Bayer, J. M. Bertrand, A. M. Boullier, J. Fabre and A. Lesquer, 1979, Evidence for late Precambrian plate tectonics in West Africa: Nature, v. 278, p. 223-227.
- Boissonnas, J. et al., 1969, On the Early Cambrian age of two late orogenic granites from west-central Ahaggar (Algerian Sahara): Canadian Journal of Earth Sciences, v. 6, p. 25-37.
- Bordet, P., 1951, Presence de laterites fossiles dans l'Atakor du Hoggar: Soc. Geol. France, C. R. no. 5-6, p. 97.
- Bordet, P., 1952, Les appareils volcaniques recents de L'Ahaggar: 19th International Geological Congress, Alger, Algeria, Monographies Regionales, First Series, No. 11, 64 p.
- Budel, J., 1955, Reliefgenerationen und Plio-Pleistozaner klimawandel im Hoggar-Gebirge (zentral Sahara): Erdkunde Bd. 9, h. 2, p. 100-115.
- Burdon, D. J., 1980, Infiltration conditions of a major sandstone aquifer around Ghat, Libya, in The Geology of Libya: Academic Press, New York, NY, v. 2, p. 595-610.
- Burollet, P. F. and R. Byramjee, 1969, Sedimentological remarks on Lower Paleozoic sandstones of south Libya, in Geology, Archaeology and Prehistory of the Southwestern Fezzan, Libya: Petrol. Explor. Soc. of Libya, p. 91-102.
- Busche, D., 1980, On the origin of the Msak Mallat and Hamadat Manghini escarpment, in The Geology of Libya: Academic Press, New York, NY, v. 3, p. 837-848.
- Cannon, P. J., 1974, Rock type discrimination using radar imagery, in Remote Sensing of Earth Resources: University of Tennessee Space Institute, Tullahoma, Tenn., v. 3, p. 339-352.
- Carpena, J., J. R. Kienast, K. Ouzegane and C. Jehanno, 1988, Evidence of the contrasted fission-track clock behavior of the apatites from In Ouzzal carbonatites (northwest Hoggar): The low-temperature thermal history of an Archean basement: Geol. Soc. of America Bull.,

v. 100, p. 1237-1243.

- Chiarelli, A., 1978, Hydrodynamic framework of eastern Algerian Sahara - influence on hydrocarbon occurrence: Am. Assoc. of Petrol. Geol. Bull., v. 62, p. 667-685.
- Cimino, J. B. and C. Elachi, 1982, Shuttle imaging radar A (SIR-A) experiment: JPL Pub. 82-77, NASA Jet Propulsion Laboratory, Pasadena, Calif., 230 p.
- Cimino, J. B., B. Holt and A. H. Richardson, 1988, The shuttle imaging radar B (SIR-B) experiment report: JPL Pub. 88-2, NASA Jet Propulsion Laboratory, Pasadena, Calif., 218 p.
- Clifford, T. N., 1970, The structural framework of Africa, in African Magmatism and Tectonics: Oliver and Boyd, Edinburgh, p. 1-26.
- Conant, L. C. and G. H. Goudarzi, 1967, Stratigraphic and tectonic framework of Libya: Am. Assoc. of Petrol. Geol. Bull., v. 51, p. 719-730.
- Daniels, C. M., 1969, The Garamantes, in Geology, Archaeology and Prehistory of the Southwestern Fezzan, Libya: Petrol. Explor. Soc. of Libya, p. 31-52.
- Elachi, C. et al., 1982, Shuttle imaging radar experiment: Science, v. 218, p. 996-1003.
- Ferrara, G. and M. Gravelle, 1966, Radiometric ages from western Ahaggar (Sahara) suggesting an eastern limit for the West African craton: Earth and Planetary Science Letters, v. 1, p. 319-324.
- Ford, J. R., 1980, Seasat orbital radar imagery for geologic mapping: Tennessee-Kentucky-Virginia: Am. Assoc. of Petrol. Geol. Bull., v. 64, p. 2064-2094.
- Ford, J. P., J. B. Cimino and C. Elachi, 1983, Space Shuttle Columbia views the world with imaging radar: The SIR-A experiment: JPL Pub. 82-95, NASA Jet Propulsion Laboratory, Pasadena, Calif., 179 p.
- Ford, J. P., J. B. Cimino, B. Holt and M. R. Ruzek, 1986, Shuttle imaging radar views the Earth from Challenger: The SIR-B experiment: JPL Pub. 86-10, NASA Jet Propulsion Laboratory, Pasadena, Calif., 135 p.
- Ford, J. P. et al., 1989, Spaceborne radar observations - A guide for Magellan radar-image analysis: JPL Pub. 89-41, NASA Jet Propulsion Laboratory, Pasadena, Calif., 126 p.

- Ghuma, M. A. and J. J. W. Rogers, 1980, Pan-African evolution in Jamahiriya and North Africa, in The Geology of Libya, v. 3, p. 1059-1064: Academic Press, New York.
- Goudarzi, G. H., 1970, Geology and mineral resources of Libya - a reconnaissance: U. S. Geol. Survey Prof. Paper 660, 104 p.
- Granath, J. W., K. A. Soofi and J. B. Mercer, 1991, Applications of SAR in structural modeling of the central ranges thrust belt, Irian Jaya, Indonesia: Presented at the Eighth Thematic Conference on Geologic Remote Sensing, Denver, Colorado, p. 105-116.
- Graziosi, P., 1969, Prehistory of southwestern Libya, in Geology, Archaeology and Prehistory of the Southwestern Fezzan, Libya: Petrol. Explor. Soc. of Libya, p. 3-20.
- Grunert, J. and D. Busche, 1980, Large-scale fossil landslides at the Msak Mallat and Hamadat Manghini escarpment, in The Geology of Libya: Academic Press, New York, NY, v. 3, p. 849-860.
- Harding, T. P., 1974, Petroleum traps associated with wrench faults: Am. Assoc. Petrol. Geol. Bull., v. 58, p. 1209-1304.
- Klitzsch, E., 1969, Stratigraphic section from the type areas of Silurian and Devonian strata at western Murzuk basin (Libya), in Geology, Archaeology and Prehistory of the Southwestern Fezzan, Libya: Petrol. Explor. Soc. of Libya, p. 83-90.
- Klitzsch, E. and D. W. Baird, 1969, Stratigraphy and paleohydrology of the Germa (Jarma) area southwest Libya, in Geology, Archaeology and Prehistory of the Southwestern Fezzan, Libya: Petrol. Explor. Soc. of Libya, p. 67-80.
- Kubiena, W. L., 1955, Ube de braunlehmrelikte des Atakor (Hoggar-Gebrige, zentral Sahara): Erdkunde Bd. 9, h. 2, p. 115-132.
- Lancelot, J., A. Vitrac and C. J. Allegre, 1976, Uranium and lead isotopic dating with grain-by-grain zircon analysis: A study of complex geological history with a single rock: Earth and Planetary Science Letters, v. 29, p. 357-366.
- Lelubre, M., 1952, L'Antecambrien de L'Ahaggar (Sahara Central): 19th International Geological Congress, Alger, Algeria, Monographies Regionales, First Series, No. 6, 148 p.

- Lillesand, T. M. and R. W. Kiefer, 1987, Remote Sensing and Image Interpretation: John Wiley & Sons, New York, NY, 721 p.
- Lorenz, J. C., 1980, Late Jurassic-Early Cretaceous sedimentation and tectonics of the Murzuq basin, southwestern Libya, in The Geology of Libya: Academic Press, New York, NY, v. 2, p. 383-392.
- Lorenz, J. C., 1987, Mixed fluvial systems of the Messak Sandstone, a deposit of the Nubian lithofacies, southwestern Libya: Sedimentary Geology, v. 54, p. 245-264.
- Maley, J., 1977, Palaeoclimates of central Sahara during the early Holocene: Nature, v. 269, p. 573-577.
- Massa, D., M. Ruhland and J. Thouvenin, 1972, Structure et fracturation du champ d'Hassi-Messaoud (Algerie): Revue du L'Institut Francais du Petrole, Juil-Aout, 1972, p. 489-713.
- Mori, F., 1969, Prehistoric cultures in Tadrart Acacus, Libyan Sahara, in Geology, Archaeology, and Prehistory of the Southwestern Fezzan, Libya: Petrol. Explor. Soc. of Libya, p. 21-30.
- Morten, L., P. L. Rossi, M. Bondi and A. O. Brunfelt, 1980, High-pressure megacrysts in basaltic lavas from Djanet Oasis, eastern Hoggar, Algerian Sahara, in The Geology of Libya: Academic Press, New York, NY, v. 3, p. 1065-1075.
- Mountjoy, A. B. and D. Hilling, 1988, Africa: Geography and Development: Hutchinson Ltd., London, 462 p.
- Muller-Feuga, R., 1954, Contribution a l'etude de la geologie, de la petrographie et des ressources hydrauliques et minerales du Fezzan: Annales de Mines et de la Geologie, Tunisie, Tunis, No. 12, 354 p.
- Pachur, H. J., 1980, Climatic history in the Late Quaternary in southern Libya and the western Libyan desert, in The Geology of Libya: Academic Press, New York, NY, v.3, p. 781-788.
- Pesce, A., 1968, Gemini space photographs of Libya and Tibesti - a geological and geographical analysis: Petrol. Explor. Soc. of Libya, 81 p.
- Sabins, F. F., Jr., 1980, Seasat radar images of San Andreas Fault, California: Am. Assoc. of Petrol. Geol. Bull., v. 64, p. 619-628.

- Sabins, F. F., Jr., 1983, Geologic interpretation of Space Shuttle radar images of Indonesia: Am. Assoc. of Petrol. Geol. Bull., v. 67, p. 2076-2099.
- Salop, L. J., 1983, Geological Evolution of the Earth During the Precambrian: Springer-Verlag, New York, NY, 459 p.
- Schatsky, N. S., 1960, Principles of Late Precambrian stratigraphy and the scope of the Riphean Group: Rept. 21st International Geological Congress, Part 8, p. 7-17.
- Schultejann, P. A., 1985, Structural trends in Borrego Valley, California: Interpretations from SIR-A and Seasat SAR: Photogrammetric Engineering and Remote Sensing, v. 51, p. 1616-1624.
- Schurmann, H. M. E., 1974, The Precambrian in North Africa: E. J. Brill, Leiden, Netherlands, 351 p.
- Short, N. M. and R. W. Blair Jr., eds., 1986, Geomorphology from Space: NASA SP-486, U. S. Govt. Printing Office, Washington, D. C., 717 p.
- Sunday Oklahoman, The, 1992, Shuttle finds desert Atlantis lost in Oman: The Sunday Oklahoman, Feb. 9, p. 4.
- Vincent, P. M., 1970, The evolution of the Tibesti Volcanic Province, eastern Sahara, in African Magmatism and Tectonics: Oliver and Boyd, Edinburgh, p. 301-319.
- Vos, R. G., 1981, Deltaic sedimentation in the Devonian of western Libya: Sedimentary Geology, v. 29, p. 67-88.
- Whitbread, T. and G. Kelling, 1982, Mrar Formation of western Libya - evolution of an Early Carboniferous delta system: Am. Assoc. of Petrol. Geol., v. 66, p. 1091-1107.
- Wilcox, R. E., T. P. Harding and D. R. Seely, 1973, Basic wrench tectonics: Am. Assoc. Petrol. Geol. Bull., v. 57, p. 74-96.
- Ziegert, H., 1966, Climatic changes and paleolithic industries in eastern Fezzan, Libya, in A Guidebook to the Geology and Prehistory of South-Central Libya and Northern Chad: Petrol. Explor. Soc. of Libya, p. 65-67.

APPENDIXES

APPENDIX A

GLOSSARY OF SELECTED ARABIC TERMS

Adrar	Mountain
Bir	Well
Djebel, Jebel	Mountain range
Dor	Group of hills; mountain range
Erg	Sand sea
Ennedi, Enneri	Valley, river bed
Gargaf	Featureless sandstone plateau
Guelta	Small swamp; rockpool
Hamada, hamadat	Rocky desert plateau
Iguidi	Dune massif
Oued	Valley; dry watercourse; wadi
Sarir	Gravel plain
Sebkha	Salt lake; salt flat
Tadrart	Mountain; mountain massif
Tarso	High plateau
Tassili	Great ravined sandstone plateau
Tehi	Pass
Wadi	Valley; dry watercourse; oued

(from Pesce, A., 1968.)

APPENDIX B

MAPS USED IN INTERPRETATIONS

Exploration Fabric of Africa (Geologic Map), 1989,
1:5,000,000, 2 panels: ERICO Petroleum Information
Ltd., PetroQuest International Inc. and Colourmap
Scanning Ltd., London.

Geological Map of Africa, 1963, 1:5,000,000, Sheets 1 and 2:
Unesco and Assoc. of African Geol. Surveys (ASGA).

International Tectonic Map of Africa, 1968, 1:5,000,000,
Sheets 1 and 2: Unesco and Assoc. of African Geol.
Surveys (ASGA).

Geologic Map of Libya, 1964, 1:2,000,000: U. S. Geological
Survey Misc. Geologic Invest. Map I-350 A; also
included in USGS Prof. Paper 660 (1970).

Also used were the following topographic maps from the
Defense Mapping Agency Aerospace Center, St. Louis Air Force
Station, Missouri, 63118.

<u>Map No.</u>	<u>Date</u>	<u>Scale</u>	<u>Area</u>
ONC J-3	1975	1:1,000,000	Southern Algeria
ONC H-3	1984	1:1,000,000	E. Algeria-W. Libya
TPC H-3C	1980	1:500,000	Southwestern Libya
TPC H-3D	1981	1:500,000	Southeastern Algeria
TPC J-3A	1989	1:500,000	Southern Algeria
TPC J-3B	1989	1:500,000	Southern Algeria
TPC J-3D	1989	1:500,000	Eastern Mali

VITA⁹

Joseph Andrew Ontko, Jr.

Candidate for the Degree of

Master of Science

Thesis: INTERPRETATION OF RADAR IMAGERY FROM SPACE SHUTTLE
COLUMBIA OVER SOUTHERN ALGERIA AND SOUTHWESTERN
LIBYA

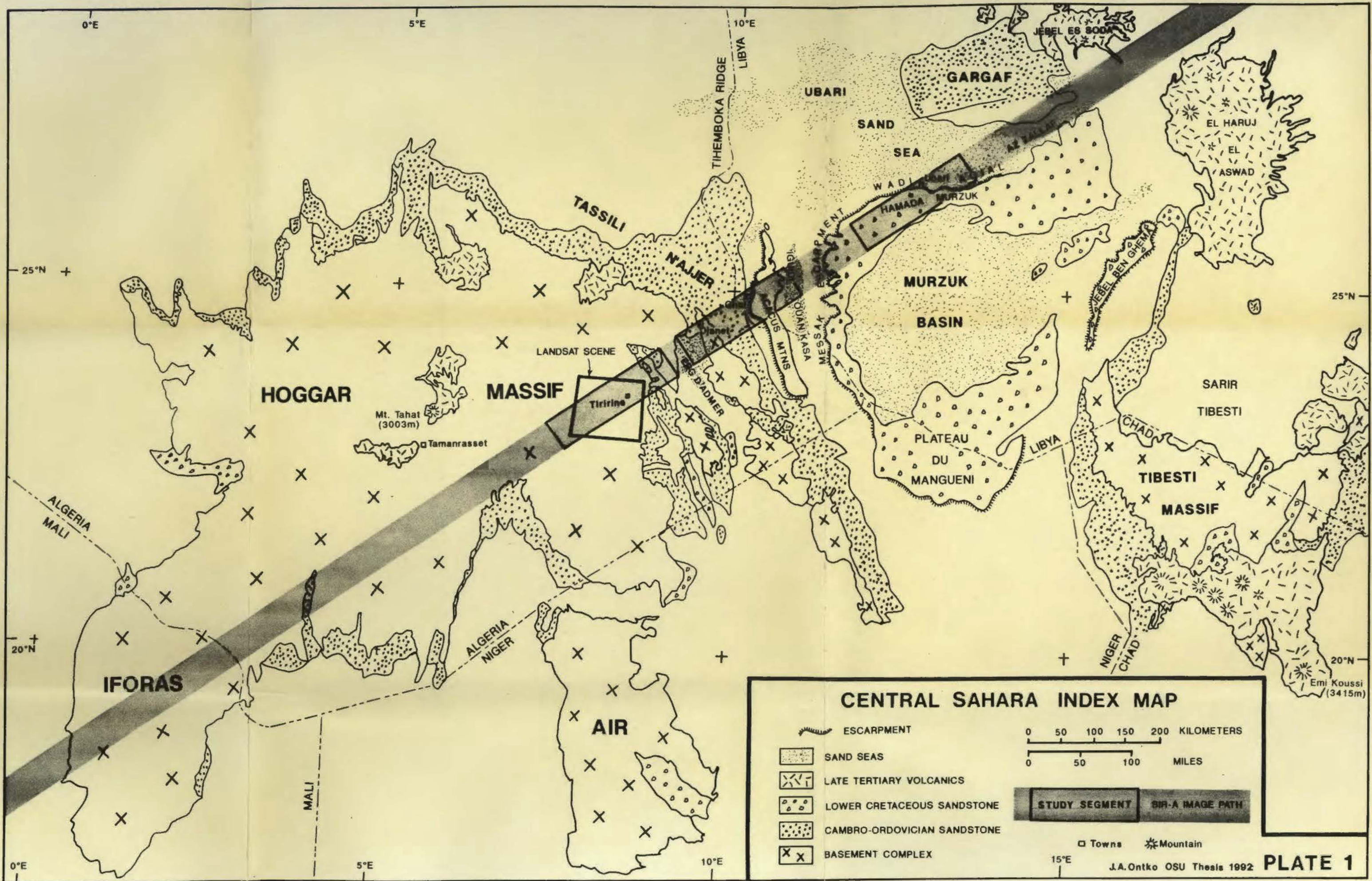
Major Field: Geology

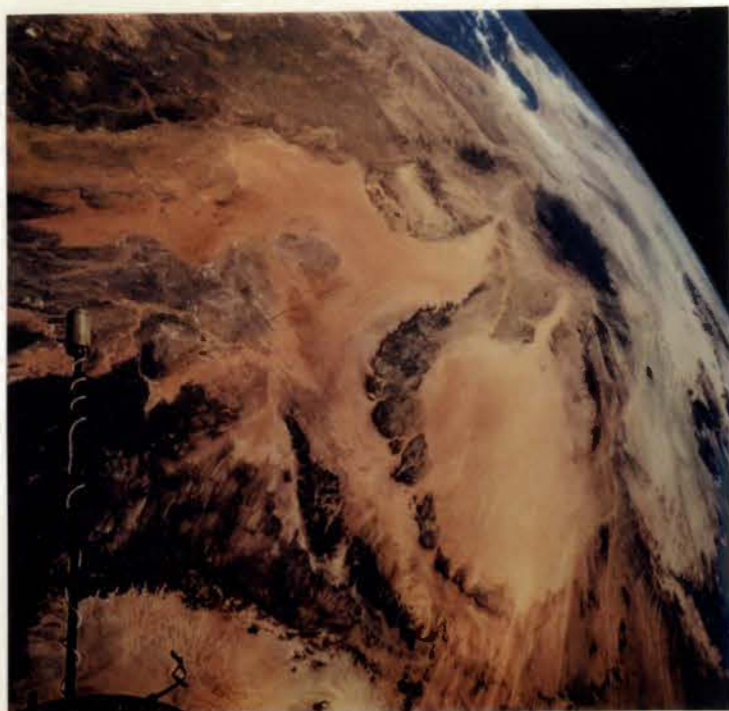
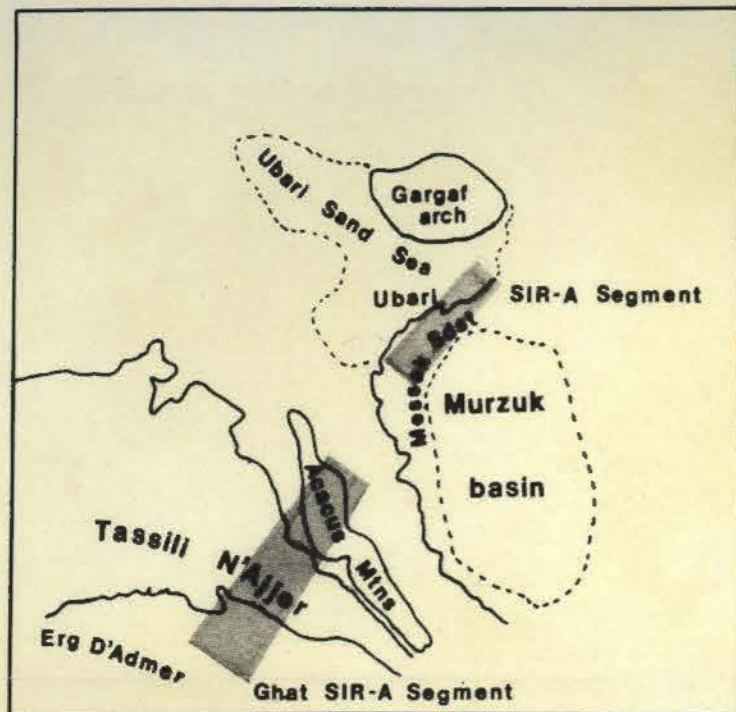
Biographical:

Personal Data: Born in Madison, Wisconsin, April 20,
1956, the son of Dr. Joseph Andrew and Carol
Ontko.

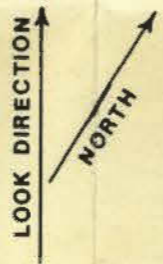
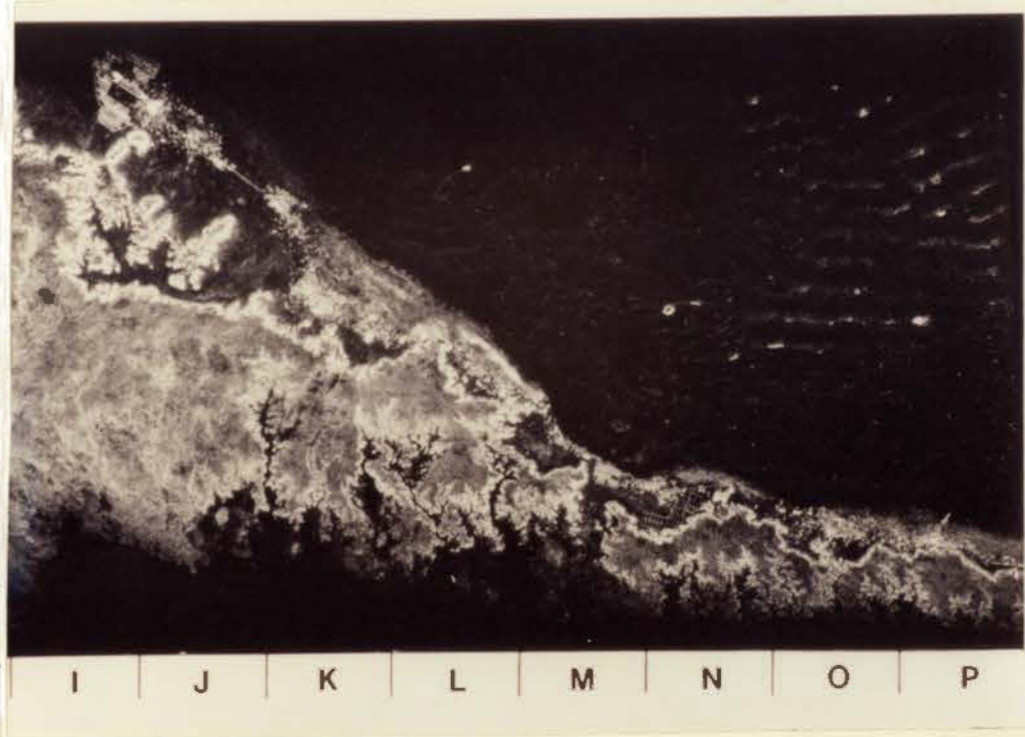
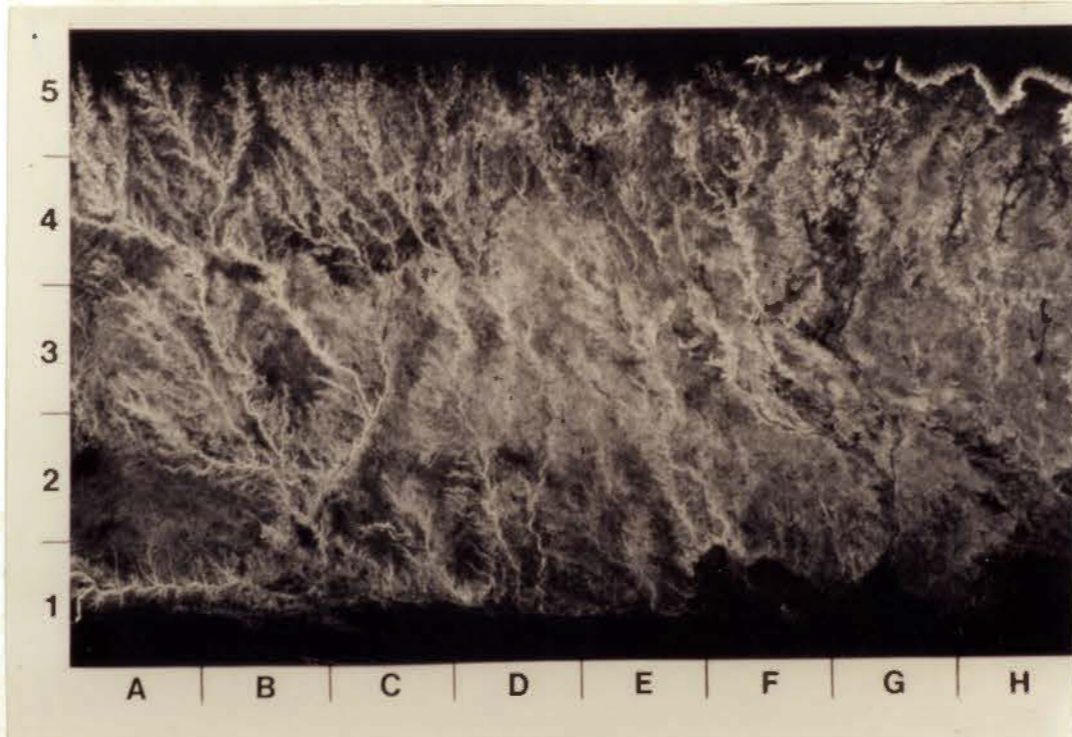
Education: Graduated from Northeast High School,
Oklahoma City, Oklahoma, May, 1974; received
Bachelor of Science Degree in Geology from
Oklahoma State University, Stillwater, Oklahoma,
December, 1978; completed requirements for the
Master of Science Degree at Oklahoma State
University in July, 1992.

Professional Experience: Geologist, MASERA
Corporation, August, 1990 to March, 1992;
Consulting Geologist, February, 1984 to July,
1990; Geologist, Bogert Oil Company, September,
1982 to January, 1984; Geologist, Bracken
Exploration

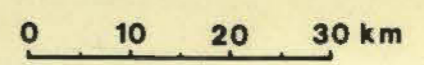


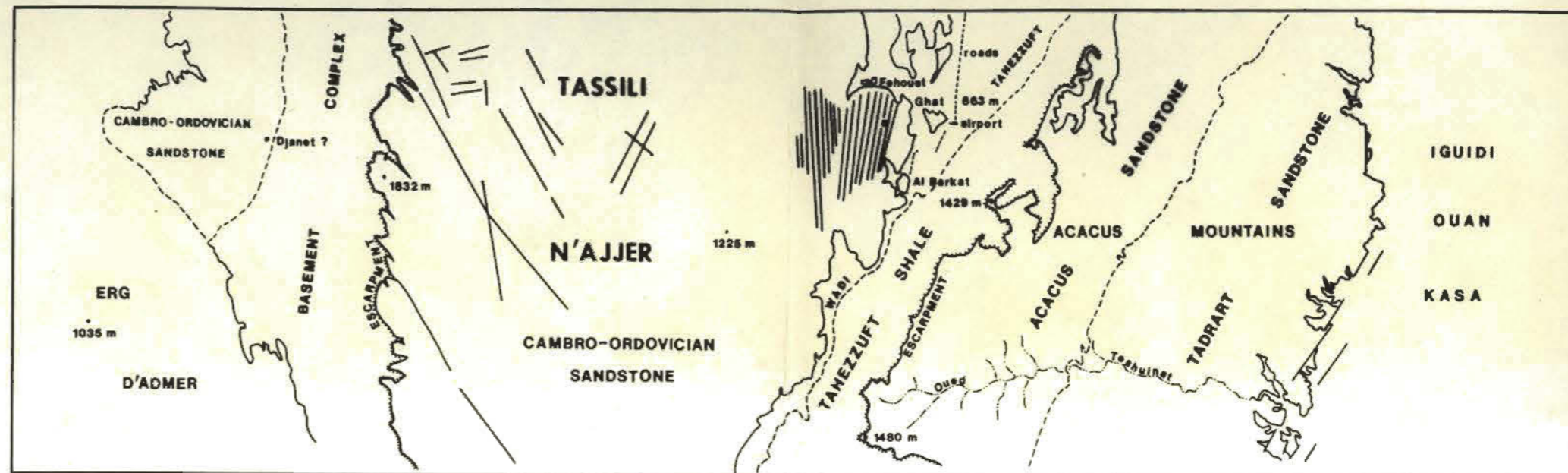
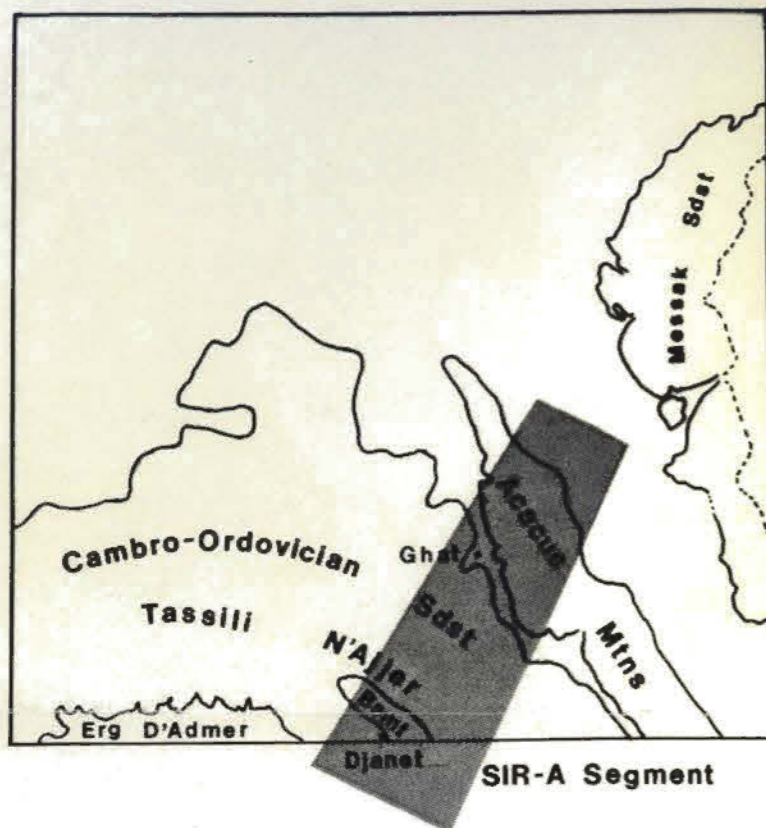


GEMINI XI PHOTOGRAPH
 No. S-66-54525
 Sept. 14, 1966
 Altitude 324 km

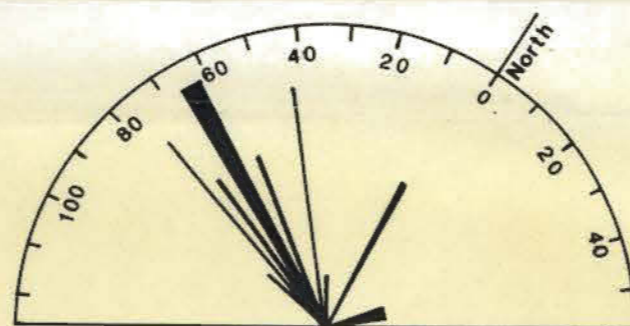
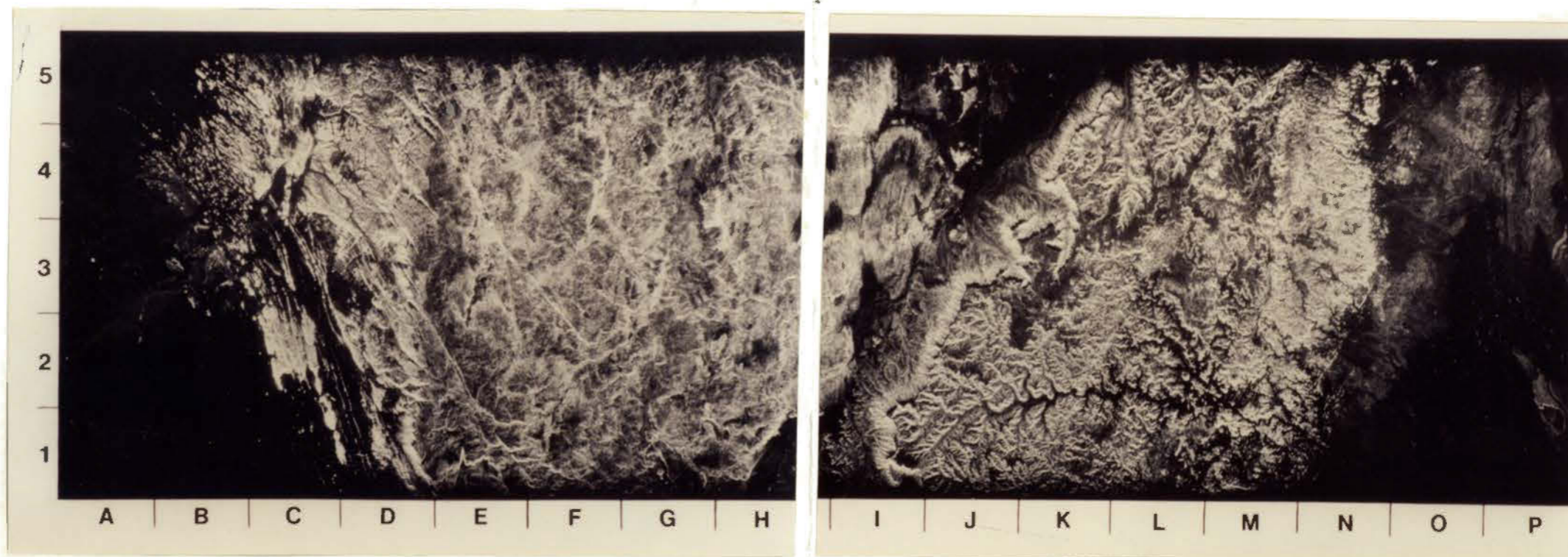


**UBARI SIR-A SEGMENT
 LIBYA**





GEMINI XI PHOTOGRAPH
No. S-66-54773
Sept. 14, 1966
Altitude 326 km

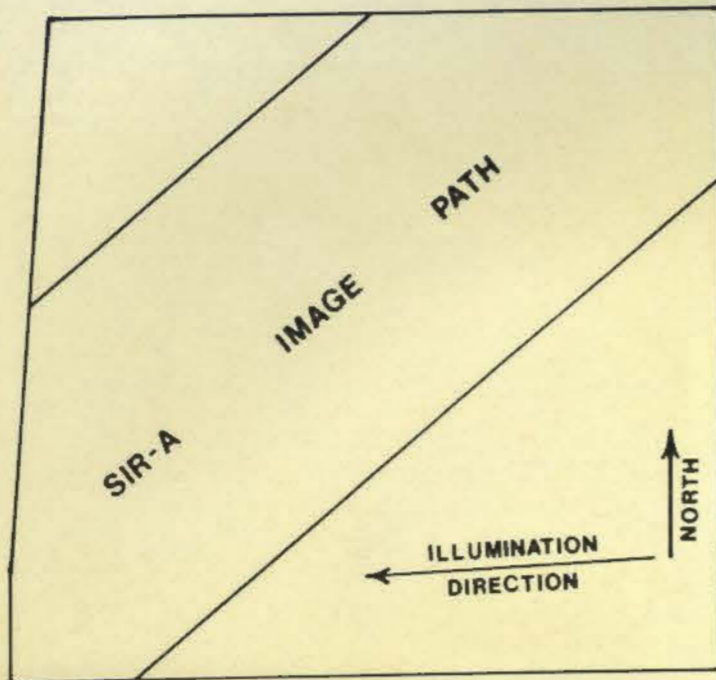


Rose Diagram of Major Lineaments in West Tassili N'ajjer C-Ord. Sdst (D-G).



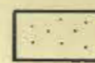

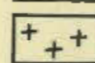


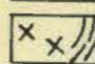



GHAT SIR-A SEGMENT
LIBYA & ALGERIA

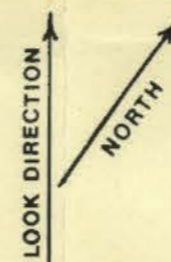
0 10 20 30 km



LANDSAT TM SCENE
No. 50141-09211
July 20, 1984



-  SAND &/or FLUVIAL DEPOSITS
-  CAMBRO-ORDOVICIAN SANDSTONE
-  PAN-AFRICAN GRANITE
-  SCHIST BELTS
-  METAMORPHIC ROCKS with TRENDS
-  HIGH-GRADE METAMORPHIC &/or GRANITIC ROCKS
-  FOLDS
-  DIKES
-  FAULTS



**TIRIRINE SIR-A SEGMENT
ALGERIA**

0 10 20 30 km